The Astrophysical Journal, 764:184 (14pp), 2013 February 20 doi:10.1088/0004-637X/764/2/184

REVISITING THE SCALING RELATIONS OF BLACK HOLE MASSES AND HOST GALAXY PROPERTIES

Nicholas J. McConnell[1,2] and Chung-Pei Ma[2]
[1] Institute for Astronomy, University of Hawaii at Manoa, Honolulu, HI, USA; nmcc@ifa.hawaii.edu
[2] Department of Astronomy, University of California at Berkeley, Berkeley, CA, USA; cpma@berkeley.edu
Received 2012 August 26; accepted 2013 January 8; published 2013 February 5

ABSTRACT

New kinematic data and modeling efforts in the past few years have substantially expanded and revised dynamical measurements of black hole masses ($M_\bullet$) at the centers of nearby galaxies. Here we compile an updated sample of 72 black holes and their host galaxies, and present revised scaling relations between $M_\bullet$ and stellar velocity dispersion (σ), V-band luminosity (L), and bulge stellar mass ($M_{\rm bulge}$), for different galaxy subsamples. Our best-fitting power-law relations for the full galaxy sample are $\log_{10}(M_\bullet) = 8.32 + 5.64\log_{10}(\sigma/200\,{\rm km\,s^{-1}})$, $\log_{10}(M_\bullet) = 9.23 + 1.11\log_{10}(L/10^{11}\,L_\odot)$, and $\log_{10}(M_\bullet) = 8.46 + 1.05\log_{10}(M_{\rm bulge}/10^{11}\,M_\odot)$. A log-quadratic fit to the $M_\bullet$–σ relation with an additional term of $\beta_2\,[\log_{10}(\sigma/200\,{\rm km\,s^{-1}})]^2$ gives $\beta_2 = 1.68 \pm 1.82$ and does not decrease the intrinsic scatter in $M_\bullet$. Including 92 additional upper limits on $M_\bullet$ does not change the slope of the $M_\bullet$–σ relation. When the early- and late-type galaxies are fit separately, we obtain similar slopes of 5.20 and 5.06 for the $M_\bullet$–σ relation but significantly different intercepts—$M_\bullet$ in early-type galaxies are about two times higher than in late types at a given sigma. Within early-type galaxies, our fits to $M_\bullet(\sigma)$ give $M_\bullet$ that is about two times higher in galaxies with central core profiles than those with central power-law profiles. Our $M_\bullet$–L and $M_\bullet$–$M_{\rm bulge}$ relations for early-type galaxies are similar to those from earlier compilations, and core and power-law galaxies yield similar L- and $M_{\rm bulge}$-based predictions for $M_\bullet$. When the conventional quadrature method is used to determine the intrinsic scatter in $M_\bullet$, our data set shows weak evidence for increased scatter at $M_{\rm bulge} < 10^{11}\,M_\odot$ or $L_V < 10^{10.3}\,L_\odot$, while the scatter stays constant for $10^{11} < M_{\rm bulge} < 10^{12.3}\,M_\odot$ and $10^{10.3} < L_V < 10^{11.5}\,L_\odot$. A Bayesian analysis indicates that a larger sample of $M_\bullet$ measurements would be needed to detect any statistically significant trend in the scatter with galaxy properties.

Key words: galaxies: nuclei – galaxies: statistics

Online-only material: color figures

1. INTRODUCTION

Empirical correlations between the masses, $M_\bullet$, of supermassive black holes and different properties of their host galaxies have proliferated in the past decade. Power-law fits to these correlations provide efficient means to estimate $M_\bullet$ in large samples of galaxies, or in individual objects with insufficient data to measure $M_\bullet$ from the dynamics of stars, gas, or masers.

Correlations between black hole masses and numerous properties of their host galaxies have been explored in the literature. These include scaling relations between $M_\bullet$ and stellar velocity dispersion (e.g., Ferrarese & Merritt 2000; Gebhardt et al. 2000; Merritt & Ferrarese 2001; Tremaine et al. 2002; Wyithe 2006a, 2006b; Hu 2008; Gültekin et al. 2009a, hereafter G09; Schulze & Gebhardt 2011; McConnell et al. 2011a; Graham et al. 2011; Beifiori et al. 2012, hereafter B12) and between $M_\bullet$ and the stellar mass of the bulge (e.g., Magorrian et al. 1998; Marconi & Hunt 2003; Häring & Rix 2004; Hu 2009; Sani et al. 2011; B12). Various scaling relations between $M_\bullet$ and the photometric properties of the galaxy have also been examined: bulge optical luminosity (e.g., Kormendy & Richstone 1995; Kormendy & Gebhardt 2001; G09; Schulze & Gebhardt 2011; McConnell et al. 2011a; B12), bulge near-infrared luminosity (e.g., Marconi & Hunt 2003; McLure & Dunlop 2002, 2004; Graham 2007; Hu 2009; Sani et al. 2011), total luminosity (e.g., Kormendy & Gebhardt 2001; Kormendy et al. 2011; B12), and bulge concentration or Sérsic index (e.g., Graham et al. 2001; Graham & Driver 2007; B12). On a larger scale, correlations between $M_\bullet$ and the circular velocity or dynamical mass of the dark matter halo have been reported as well as disputed (e.g., Ferrarese 2002; Baes et al. 2003; Zasov et al. 2005; Kormendy & Bender 2011; Volonteri et al. 2011; B12). More recently, $M_\bullet$ has been found to correlate with the number and total mass of globular clusters in the host galaxy (e.g., Burkert & Tremaine 2010; Harris & Harris 2011; Sadoun & Colin 2012). In early-type galaxies with core profiles, Lauer et al. (2007a) and Kormendy & Bender (2009) have explored correlations between $M_\bullet$ and the core radius, or the total "light deficit" of the core relative to a Sérsic profile.

Recent kinematic data and modeling efforts have substantially expanded the various samples used in all of the studies above. In this paper, we take advantage of these developments, presenting an updated compilation of 72 black holes and their host galaxies and providing new scaling relations. Our sample is a significant update from two recent compilations by G09 and Graham et al. (2011). Compared with the 49 objects in G09, 27 black holes in our present sample are new measurements, and 18 masses are updated values from better data and/or more sophisticated modeling. Compared with the 64 objects in Graham et al. (2011) (an update of Graham 2008), 35 of our black hole masses are new or updates. The G09 and Graham (2008) samples differ by only a few galaxies, based on the authors' respective judgments about which dynamical measurements are reliable. The most significant updates in our sample are galaxies with extremely high $M_\bullet$ (Shen & Gebhardt 2010; Gebhardt et al. 2011; McConnell et al. 2011a, 2011b, 2012; Rusli 2012) and galaxies with some of the smallest observed central black holes (Greene et al. 2010; Nowak et al. 2010; Kormendy et al. 2011; Kuo et al. 2011). Our present sample includes updated distances to 44 galaxies, mostly based on surface brightness fluctuation measurements (Tonry et al. 2001; Blakeslee et al. 2009, 2010).

We focus on three frequently studied scaling relations: $M_\bullet$ versus stellar velocity dispersion (σ), V-band bulge luminosity

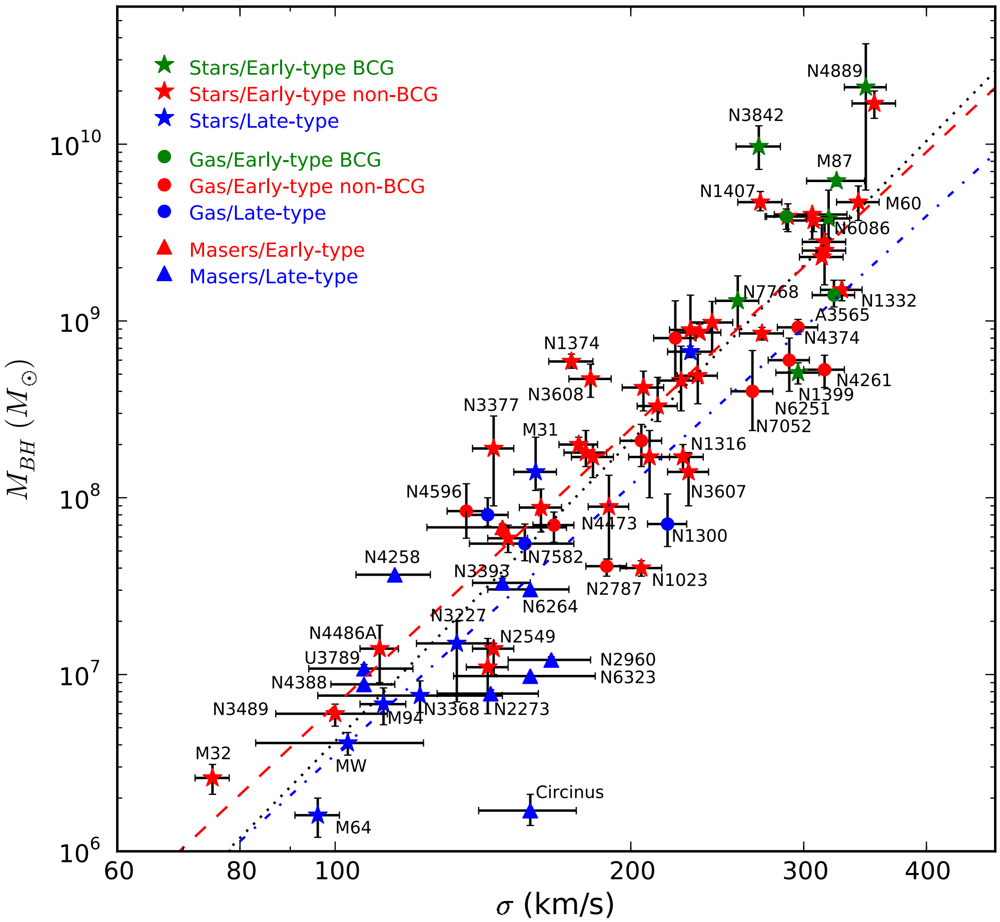

Figure 1. $M_\bullet$–σ relation for our full sample of 72 galaxies listed in Table 3 and at http://blackhole.berkeley.edu. Brightest cluster galaxies (BCGs) that are also the central galaxies of their clusters are plotted in green, other elliptical and S0 galaxies are plotted in red, and late-type spiral galaxies are plotted in blue. NGC 1316 is the most luminous galaxy in the Fornax cluster, but it lies at the cluster outskirts; the green symbol here labels the central galaxy NGC 1399. M87 lies near the center of the Virgo cluster, whereas NGC 4472 (M49) lies ∼1 Mpc to the south. The black hole masses are measured using the dynamics of masers (triangles), stars (stars), or gas (circles). Error bars indicate 68% confidence intervals. For most of the maser galaxies, the error bars in $M_\bullet$ are smaller than the plotted symbol. The black dotted line shows the best-fitting power law for the entire sample: $\log_{10}(M_\bullet/M_\odot) = 8.32+5.64\log_{10}(\sigma/200\,\mathrm{km\,s^{-1}})$. When early-type and late-type galaxies are fit separately, the resulting power laws are $\log_{10}(M_\bullet/M_\odot) = 8.39+5.20\log_{10}(\sigma/200\,\mathrm{km\,s^{-1}})$ for the early type (red dashed line), and $\log_{10}(M_\bullet/M_\odot) = 8.07+5.06\log_{10}(\sigma/200\,\mathrm{km\,s^{-1}})$ for the late type (blue dot-dashed line). The plotted values of σ are derived using kinematic data over the radii $r_{\rm inf} < r < r_{\rm eff}$.

(A color version of this figure is available in the online journal.)

(L), and stellar bulge mass ($M_{\rm bulge}$). As reported below, our new compilation results in a significantly steeper power law for the $M_\bullet$–σ relation than in G09 and the recent investigation by B12, who combined the previous sample of 49 black holes from G09 with a larger sample of upper limits on $M_\bullet$ from Beifiori et al. (2009). We still find a steeper power law than G09 or B12 when we include these upper limits in our fit to the $M_\bullet$–σ relation. We have performed a quadratic fit to $M_\bullet(\sigma)$ and find a marginal amount of upward curvature, similar to previous investigations (Wyithe 2006a, 2006b; G09).

Another important measurable quantity is the intrinsic or cosmic scatter in $M_\bullet$ for fixed galaxy properties. Quantifying the scatter in $M_\bullet$ is useful for identifying the tightest correlations from which to predict $M_\bullet$ and for testing different scenarios of galaxy and black hole growth. In particular, models of stochastic black hole and galaxy growth via hierarchical merging predict decreasing scatter in $M_\bullet$ as galaxy mass increases (e.g., Peng 2007; Jahnke & Macciò 2011). Previous empirical studies of the black hole scaling relations have estimated the intrinsic scatter in $M_\bullet$ as a single value for the entire sample. Herein, we take advantage of our larger sample to estimate the scatter as a function of σ, L, and $M_{\rm bulge}$.

In Section 2 we summarize our updated compilation of 72 black hole mass measurements and 35 bulge masses from dynamical studies. In Section 3 we present fits to the $M_\bullet$–σ, $M_\bullet$–L, and $M_\bullet$–$M_{\rm bulge}$ relations and highlight subsamples that yield interesting variations in the best-fit power laws. In particular, we examine different cuts in σ, L, and $M_{\rm bulge}$, as well as cuts based on galaxies' morphologies and surface brightness profiles. In Section 4 we discuss the scatter in $M_\bullet$ and its dependence on σ, L, and $M_{\rm bulge}$. In Section 5 we discuss how our analysis of galaxy subsamples may be beneficial for various applications of the black hole scaling relations.

Our full sample of black hole masses and galaxy properties is available online at http://blackhole.berkeley.edu. This database will be updated as new results are published. Investigators are encouraged to use this online database and inform us of updates.

2. AN UPDATED BLACK HOLE AND GALAXY SAMPLE

Our full sample of 72 black hole masses and their host galaxy properties are listed in Table 3, which appears at the end of this paper. The corresponding $M_\bullet$ versus σ, L, and $M_{\rm bulge}$ are plotted in Figures 1–3. This sample is an update of our previous compilation of 67 dynamical black hole measurements,

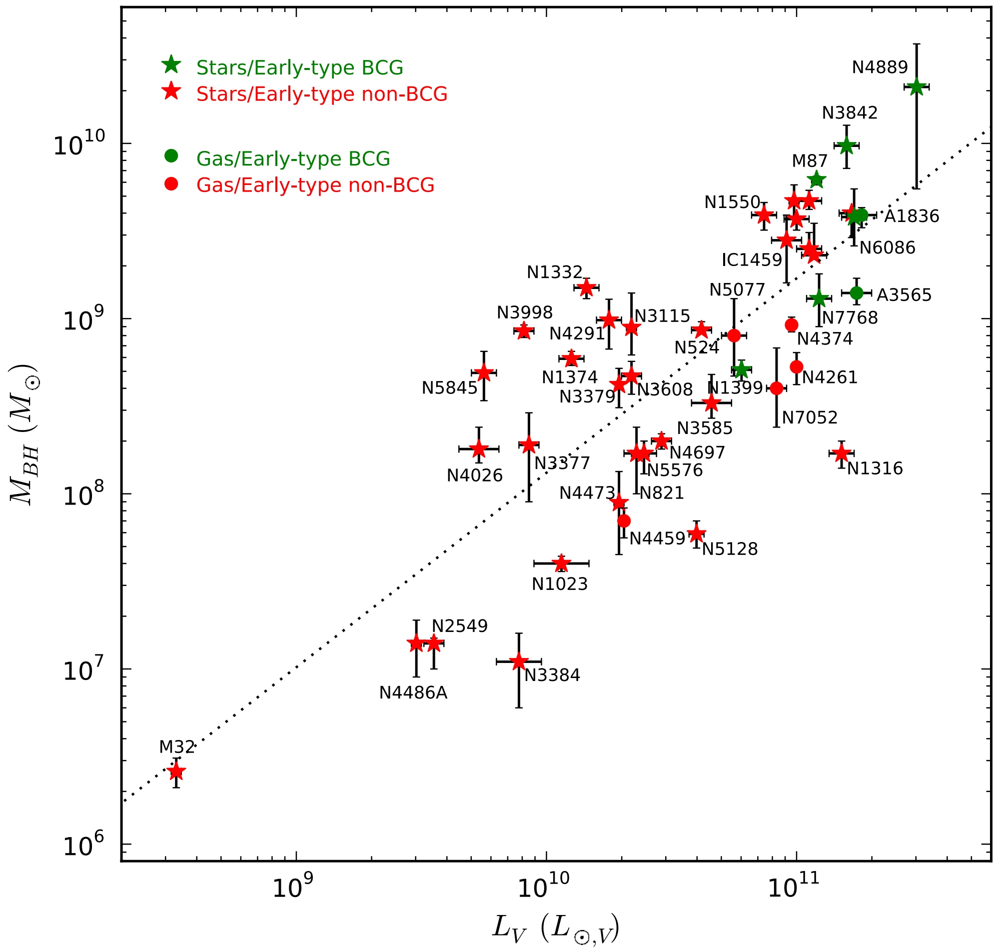

Figure 2. $M_\bullet$–L relation for the 44 early-type galaxies with reliable measurements of the V-band bulge luminosity in our sample. The symbols are the same as in Figure 1. The black line represents the best-fitting power-law $\log_{10}(M_\bullet/M_\odot) = 9.23 + 1.11 \log_{10}(L_v/10^{11} L_\odot)$.
(A color version of this figure is available in the online journal.)

presented in the supplementary materials to McConnell et al. (2011a). The current sample includes one new measurement of $M_\bullet$ from McConnell et al. (2012), seven new measurements from Rusli (2012), and two updated measurements (NGC 4594, Jardel et al. 2011; NGC 3998, Walsh et al. 2012). For NGC 5128 (Cen A), we have adopted the value $M_\bullet = 5.9^{+1.1}_{-1.0} \times 10^7 M_\odot$ (at a distance of 4.1 Mpc) from Cappellari et al. (2009).

We have removed three galaxies whose original measurements have exceptional complications. Lodato & Bertin (2003) measured non-Keplerian maser velocities in NGC 1068 and estimated $M_\bullet$ by modeling a self-gravitating disk. Still, other physical processes might reproduce the observed maser motions. Atkinson et al. (2005) reported a measurement of $M_\bullet$ in NGC 2748 but noted that heavy extinction could corrupt their attempt to locate the center of the nuclear gas disk. Gebhardt et al. (2003) justified classifying the central point source of NGC 7457 as an active galactic nucleus, but their arguments permit the central mass to be shared by an accreting black hole and a nuclear star cluster.

Additionally, we have updated the distances to 44 galaxies in our sample. For 41 galaxies, we adopt surface brightness fluctuation measurements from Tonry et al. (2001) and Blakeslee et al. (2009), with the corrections suggested by Blakeslee et al. (2010). For M31 and M32, we adopt the Cepheid variable distance of 0.73 Mpc from Vilardell et al. (2007). For NGC 4342, we adopt the distance of 23 Mpc from Bogdán et al. (2012). Other measured quantities are scaled accordingly: $M_\bullet \propto D$, $L \propto D^2$, and $M_{\rm bulge} \propto D$. Table 3 includes the updated values for all quantities. The new galaxy distances and rescaled $M_\bullet$ only have a small effect on our fits to the black hole scaling relations. For other galaxy distances, we assume $H_0 = 70\,{\rm km\,s^{-1}\,Mpc^{-1}}$, as in McConnell et al. (2011a).

For the $M_\bullet$–σ relation, we also consider upper limits for $M_\bullet$ in 89 galaxies from B12, plus three new upper limits (Schulze & Gebhardt 2011; Gültekin et al. 2011; McConnell et al. 2012). Five additional galaxies in the B12 upper limit sample have recently obtained secure measurements of $M_\bullet$ and are included in our 72-galaxy sample. As we discuss in Section 3, including upper limits results in a lower normalization (intercept) for the $M_\bullet$–σ relation but does not significantly alter the slope.

For the $M_\bullet$–σ relation, we consider two different definitions of σ. Both definitions use spatially resolved measurements of the line-of-sight velocity dispersion $\sigma(r)$ and radial velocity $v(r)$, integrated out to one effective radius ($r_{\rm eff}$):

$$\sigma^2 \equiv \frac{\int_{r_{\rm min}}^{r_{\rm eff}} [\sigma^2(r) + v^2(r)] I(r) dr}{\int_{r_{\rm min}}^{r_{\rm eff}} I(r) dr} \quad , \qquad (1)$$

where $I(r)$ is the galaxy's one-dimensional stellar surface brightness profile. In G09 and most other studies, the lower integration limit $r_{\rm min}$ is set to zero and sampled at the smallest scale allowed by the data. This definition of σ, however,

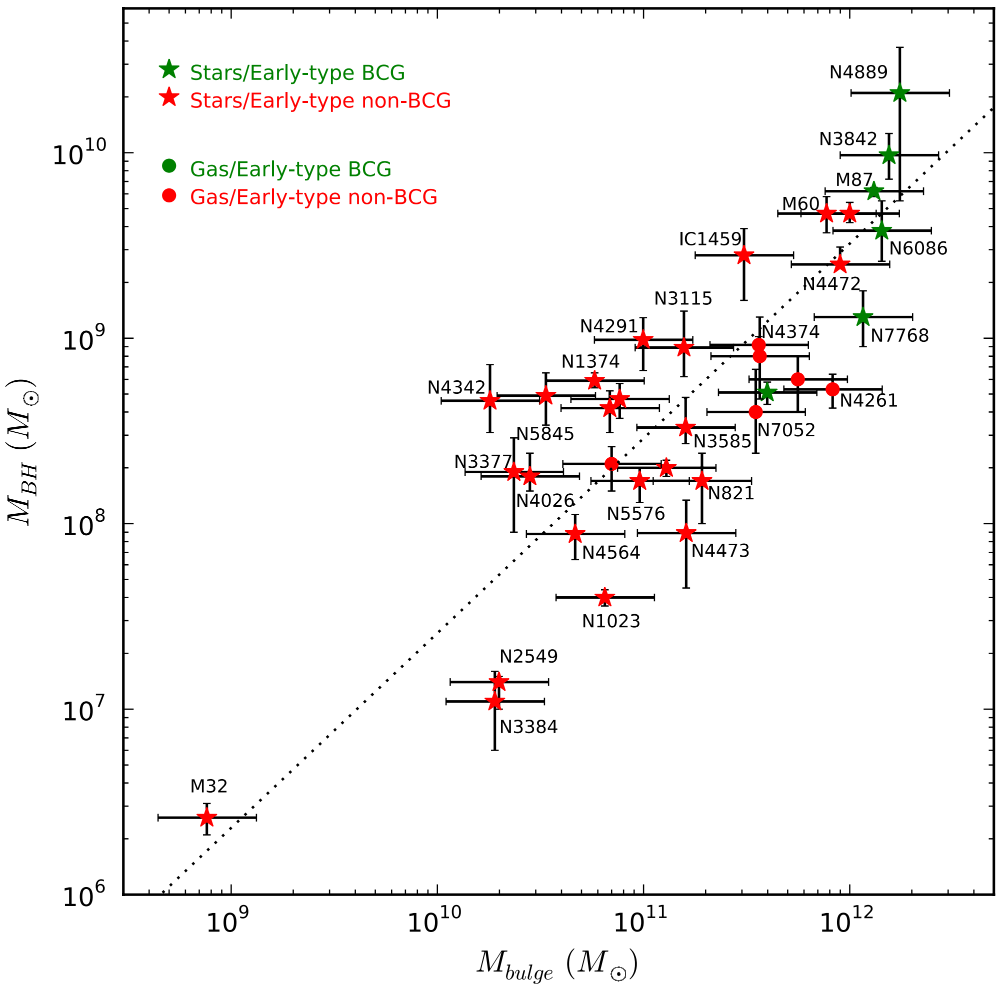

Figure 3. $M_\bullet$–$M_{\rm bulge}$ relation for the 35 early-type galaxies with dynamical measurements of the bulge stellar mass in our sample. The symbols are the same as in Figure 1. The black line represents the best-fitting power-law $\log_{10}(M_\bullet/M_\odot) = 8.46 + 1.05\,\log_{10}(M_{\rm bulge}/10^{11}\,M_\odot)$.
(A color version of this figure is available in the online journal.)

includes signal from within the black hole radius of influence, $r_{\rm inf} \equiv GM_\bullet\sigma^{-2}$. In some galaxies, particularly the most massive ellipticals, σ decreases substantially when spatially resolved data within $r_{\rm inf}$ are excluded. Setting $r_{\rm min} = r_{\rm inf}$ produces an alternative definition of σ that reflects the global structure of the galaxy and is less sensitive to angular resolution. We compare the two definitions of σ for 12 galaxies whose kinematics within $r_{\rm inf}$ are notably different from kinematics at larger radii. As shown in Table 1, excluding $r < r_{\rm inf}$ can reduce σ by up to 10%–15%. Ten of the 12 updated galaxies are massive ($\sigma > 250\,{\rm km\,s^{-1}}$ using either definition). Rusli (2012) presented seven new stellar dynamical measurements of $M_\bullet$ along with central velocity dispersions. We have used the long-slit kinematics from Rusli (2012) and references therein to derive σ according to Equation (1); our σ values appear in Tables 1 and 3 and.

For the $M_\bullet$–$M_{\rm bulge}$ relation, we have compiled the bulge stellar masses for 35 early-type galaxies. Among them, 13 bulge masses are taken from Häring & Rix (2004), who used spherical Jeans models to fit stellar kinematics. For 22 more galaxies, we multiply the V-band luminosity in Table 3 with the bulge mass-to-light ratio (M/L) derived from kinematics and dynamical modeling of stars or gas (see Table 3 for references). Where necessary, M/L is converted to V band using galaxy colors. The

Table 1
Galaxies with Multiple Definitions of σ

Galaxy	Ref.	$r_{\rm inf}$ (″)	σ (0–$r_{\rm eff}$) (km s^{-1})	σ ($r_{\rm inf}$–$r_{\rm eff}$) (km s^{-1})
IC 1459	1	0.81	340	315
NGC 1374	2	0.89	203	174
NGC 1399	3,4	0.63	337	296
NGC 1407	5	1.9	283	274
NGC 1550	6	0.78	302	289
NGC 3842	7	1.2	275	270
NGC 3998	8	0.71	286	272
NGC 4486	9	2.1	375	324
NGC 4594	10	1.2	240	230
NGC 4649	11	2.2	385	341
NGC 4889	7	1.5	360	347
NGC 7619	12	0.39	324	313
NGC 7768	7	0.14	265	257

Notes. References for kinematic data used to derive $r_{\rm inf}$ are (1) Cappellari et al. 2002; (2) D'Onofrio et al. 1995; (3) Graham et al. 1998; (4) Gebhardt et al. 2007; (5) Spolaor et al. 2008; (6) Simien & Prugniel 2000; (7) McConnell et al. 2012; (8) Walsh et al. 2012; (9) Gebhardt et al. 2011; (10) Jardel et al. 2011; (11) Pinkney et al. 2003; and (12) Pu et al. 2010. Although Rusli (2012) reports long-slit kinematic measurements for NGC 1374, the measurements from D'Onofrio et al. (1995) are more consistent with high-resolution SINFONI data in Rusli (2012).

values of $M_{\rm bulge}$ are scaled to reflect the assumed distances in Table 3.

Most of the dynamical models behind our compiled values of $M_{\rm bulge}$ have assumed that mass follows light. This assumption can be appropriate in the inner regions of galaxies, where dark matter does not contribute significantly to the total enclosed mass. Still, several measurements are based on kinematic data out to large radii. Furthermore, some galaxies exhibit contradictions between the dynamical estimates of M/L and estimates of M/L from stellar population synthesis models (e.g., Cappellari et al. 2006; Conroy & van Dokkum 2012). For this reason, we adopt a conservative approach and assign a minimum error of 0.24 dex to each value of $M_{\rm bulge}$. The corresponding confidence interval (0.58–1.74) $\times$ $M_{\rm bulge}$ spans a factor of three.

To test how well our $M_{\rm bulge}$ values represent the stellar mass of each galaxy, we also have fit the $M_\bullet$–$M_{\rm bulge}$ relation using a sample of 18 galaxies for which $M_{\rm bulge}$ is computed from the stellar mass-to-light ratio, $M_\star/L$. Our stellar $M_{\rm bulge}$ sample comprises 13 galaxies for which $M_\star/L$ is measured from dynamical models including dark matter, plus five galaxies for which $M_\star/L$ is derived from stellar population models by Conroy & van Dokkum (2012). This sample yields a slightly steeper slope of 1.34 ± 0.15 for the $M_\bullet$–$M_{\rm bulge}$ relation, versus a slope of 1.05 ± 0.11 for our 35-galaxy dynamical $M_{\rm bulge}$ sample. The stellar $M_{\rm bulge}$ sample also has substantially lower scatter in $M_\bullet$ (see Table 2).

3. BLACK HOLE SCALING RELATIONS AND FITS

In this section we present results for the fits to black hole scaling relations for the full sample of dynamically measured $M_\bullet$ listed in Table 3, the full sample of $M_\bullet$ plus 92 upper limits on $M_\bullet$, and various subsamples divided by galaxy properties.

3.1. Fitting Methods

Our power-law fit to a given sample is defined in log space by an intercept α and slope β:

$$\log_{10} M_\bullet = \alpha + \beta \log_{10} X, \quad (2)$$

where $M_\bullet$ is in units of $M_\odot$, and $X = \sigma/200\,{\rm km\,s^{-1}}$, $L/10^{11} L_\odot$, or $M_{\rm bulge}/10^{11} M_\odot$ for the three scaling relations. We have also tested a log-quadratic fit for the $M_\bullet$–σ relation:

$$\log_{10} M_\bullet = \alpha + \beta \log_{10} X + \beta_2 [\log_{10} X]^2, \quad (3)$$

where $X = \sigma/200\,{\rm km\,s^{-1}}$. Results for the quadratic fit are discussed separately in Section 3.2.6 below.

For the power-law scaling relations, we have compared three linear regression estimators: `MPFITEXY`, `LINMIX_ERR`, and `BIVAR EM`. `MPFITEXY` is a least-squares estimator by Williams et al. (2010). `LINMIX_ERR` is a Bayesian estimator by Kelly (2007). Both `MPFITEXY` and `LINMIX_ERR` consider measurement errors in two variables and include an intrinsic scatter term, ϵ_0, in $\log(M_\bullet)$. `LINMIX_ERR` can be applied to galaxy samples with upper limits for $M_\bullet$. For the $M_\bullet$–σ sample with upper limits, we also use the `BIVAR EM` algorithm in the `ASURV` software package by Lavalley et al. (1992), which implements the methods presented in Isobe et al. (1986). The `ASURV` procedures do not consider measurement errors, and we use this method primarily for comparison with B12. All three algorithms are publicly available.[3]

[3] The IDL source code for `MPFITEXY` is available at http://purl.org/mike/mpfitexy. The IDL source code for `LINMIX_ERR` and dependent scripts is available at http://idlastro.gsfc.nasa.gov/ftp/pro/math. `ASURV` is available at http://www2.astro.psu.edu/statcodes/asurv.

For each of the global scaling relations and galaxy subsamples, we obtain consistent fits from `MPFITEXY` and `LINMIX_ERR`, although `LINMIX_ERR` usually returns a slightly higher value of ϵ_0. Table 2 includes the global fitting results from both methods. In Table 2 we also include results from `LINMIX_ERR` in cases where ϵ_0 is poorly constrained by `MPFITEXY`. For the $M_\bullet$–σ relation including upper limits, the `BIVAR EM` procedure returns a lower intercept than `LINMIX_ERR`, but the slopes from the two methods are consistent within errors. Recently, Park et al. (2012) investigated the $M_\bullet$–σ relation using four linear regression estimators, including `MPFITEXY` and `LINMIX_ERR`. All four estimators yielded consistent fits to empirical data, and `MPFITEXY` and `LINMIX_ERR` behaved robustly for simulated data with large measurement errors in σ.

3.2. $M_\bullet$–σ Relation

Our fits to $M_\bullet(\sigma)$ for the entire galaxy sample and various subsamples are plotted in Figures 1 and 4(a), and summarized in Table 2.

3.2.1. Full Sample

Our full sample of 72 galaxies yields an intercept $\alpha = 8.32 \pm 0.05$ and slope $\beta = 5.64 \pm 0.32$. When upper limits are added, the sample of 164 galaxies yields $\alpha = 8.15 \pm 0.05$ and $\beta = 5.58 \pm 0.30$. The reduced intercept is a natural consequence of considering upper limits, while the slightly shallower slope is consistent within errors.

3.2.2. Early versus Late Types

Fitting early- and late-type galaxies separately yields slightly shallower slopes: $\beta = 5.20 \pm 0.36$ for early types (red dashed line in Figure 1) and $\beta = 5.06 \pm 1.16$ for late types (blue dot-dashed line). The late-type galaxies have a significantly lower intercept: $\alpha = 8.39 \pm 0.06$ versus 8.07 ± 0.21. Correspondingly, our fits predict $M_{\bullet,{\rm early}} \sim 2\,M_{\bullet,{\rm late}}$ at fixed σ. Because most of the late-type bulges have low σ, the split in intercepts leads to a steeper slope of 5.64 for the full sample.

3.2.3. Core versus Power Law

We also consider two subsamples of early-type galaxies classified by the slopes of their inner surface brightness profiles, $\gamma = -d \log I / d \log r$. Faber et al. (1997) and Lauer et al. (2007b) distinguished "power-law" galaxies with $\gamma > 0.5$ from "core" galaxies with $\gamma < 0.3$, although other studies have reported a continuous trend in γ (e.g., Ferrarese et al. 2006; Glass et al. 2011). Core galaxies tend to be more massive and luminous than power-law galaxies, and there is some evidence that $M_\bullet$ correlates with properties of the inner stellar core (Lauer et al. 2007a; Kormendy & Bender 2009). In our fits to $M_\bullet(\sigma)$, core galaxies have a significantly higher intercept than power-law galaxies (see Figure 4(a)): $\alpha = 8.53 \pm 0.11$ versus 8.24 ± 0.09. Our fits predict $M_{\bullet,{\rm core}} \sim 2\,M_{\bullet,{\rm pl}}$ at $\sigma \sim 200\,{\rm km\,s^{-1}}$, where the two populations overlap. The offset in intercepts plus the shallower slopes ($\beta \approx 4.5$–4.8) for core and power-law galaxies combine to produce a steeper slope ($\beta \approx 5.2$) for the early-type $M_\bullet$–σ relation.

3.2.4. Definitions of σ

As discussed in Section 2, the value of σ for each galaxy used in the $M_\bullet$–σ relation depends on the spatial extent of the kinematic data. Excluding data within $r_{\rm inf}$ (when resolved) has

Table 2
Power-law Fits to Black Hole Correlations

Sample	$N_{\rm gal}$	Method	α	β	ϵ_0
$M_\bullet$–σ relation					
All galaxies	72	MPFITEXY	8.32 ± 0.05	5.64 ± 0.32	0.38
All galaxies	72	LINMIX_ERR	8.31 ± 0.06	5.67 ± 0.33	0.40 ± 0.04
All + upper limits	164	ASURV	7.72 ± 0.12	5.37 ± 0.62	
All + upper limits	164	LINMIX_ERR	8.15 ± 0.05	5.58 ± 0.30	0.43 ± 0.04
All galaxies (0–$r_{\rm eff}$)	72	MPFITEXY	8.29 ± 0.05	5.48 ± 0.30	0.37
G09 data (0–$r_{\rm eff}$)	49	MPFITEXY	8.19 ± 0.06	4.12 ± 0.38	0.39
Early type	53	MPFITEXY	8.39 ± 0.06	5.20 ± 0.36	0.34
Early type (0–$r_{\rm eff}$)	53	MPFITEXY	8.36 ± 0.05	5.05 ± 0.34	0.33
Late type	19	MPFITEXY	8.07 ± 0.21	5.06 ± 1.16	0.46
Power law	18	MPFITEXY	8.24 ± 0.09	4.51 ± 0.73	0.34
Core	28	MPFITEXY	8.53 ± 0.11	4.79 ± 0.74	0.35
Core (0–$r_{\rm eff}$)	28	MPFITEXY	8.50 ± 0.11	4.63 ± 0.68	0.34
$\sigma \leqslant 200\,{\rm km\,s^{-1}}$	35	MPFITEXY	8.35 ± 0.15	5.66 ± 0.85	0.43
$\sigma > 200\,{\rm km\,s^{-1}}$	37	MPFITEXY	8.16 ± 0.13	6.76 ± 0.91	0.34
$\sigma > 200\,{\rm km\,s^{-1}}$ (0–$r_{\rm eff}$)	38	MPFITEXY	8.26 ± 0.12	5.70 ± 0.78	0.35
$\sigma \leqslant 275\,{\rm km\,s^{-1}}$	55	LINMIX_ERR	8.33 ± 0.07	5.77 ± 0.51	0.43 ± 0.05
$\sigma > 275\,{\rm km\,s^{-1}}$	17	LINMIX_ERR	7.00 ± 2.42	12.3 ± 12.6	0.34 ± 0.11
$\sigma > 275\,{\rm km\,s^{-1}}$	17	MPFITEXY	2.47 ± 3.17	35.8 ± 16.5	N/A
$\sigma > 290\,{\rm km\,s^{-1}}$ (0–$r_{\rm eff}$)	15	LINMIX_ERR	7.68 ± 1.26	7.93 ± 5.79	0.32 ± 0.11
$L \leqslant 10^{10.8}\,L_\odot$	25	MPFITEXY	8.37 ± 0.08	4.76 ± 0.55	0.33
$L > 10^{10.8}\,L_\odot$	19	MPFITEXY	8.13 ± 0.40	7.19 ± 2.25	0.37
$L > 10^{10.8}\,L_\odot$ (0–$r_{\rm eff}$)	19	MPFITEXY	8.29 ± 0.33	5.83 ± 1.75	0.36
$M_{\rm bulge} \leqslant 10^{11.5}\,M_\odot$	21	MPFITEXY	8.40 ± 0.09	5.08 ± 0.70	0.34
$M_{\rm bulge} > 10^{11.5}\,M_\odot$	14	MPFITEXY	8.52 ± 0.47	4.69 ± 2.69	0.46
$M_{\rm bulge} > 10^{11.5}\,M_\odot$ (0–$r_{\rm eff}$)	14	MPFITEXY	8.61 ± 0.40	3.80 ± 2.09	0.45
$M_\bullet$–L relation					
Early-type galaxies	44	MPFITEXY	9.23 ± 0.10	1.11 ± 0.13	0.49
Early-type galaxies	44	LINMIX_ERR	9.23 ± 0.10	1.11 ± 0.14	0.52 ± 0.06
G09 data (early type)	32	MPFITEXY	9.01 ± 0.10	1.17 ± 0.12	0.36
Power law	12	MPFITEXY	9.36 ± 0.72	1.19 ± 0.67	0.68
Core	27	MPFITEXY	9.28 ± 0.09	1.17 ± 0.22	0.39
$L \leqslant 10^{10.8}\,L_\odot$	25	MPFITEXY	9.10 ± 0.23	0.98 ± 0.20	0.54
$L > 10^{10.8}\,L_\odot$	19	MPFITEXY	9.27 ± 0.13	1.12 ± 0.82	0.47
$M_{\rm bulge} \leqslant 10^{11.5}\,M_\odot$	18	MPFITEXY	9.25 ± 0.24	1.13 ± 0.23	0.47
$M_{\rm bulge} > 10^{11.5}\,M_\odot$	13	MPFITEXY	9.24 ± 0.10	2.49 ± 0.67	0.30
$M_\bullet$–$M_{\rm bulge}$ relation					
Dynamical masses	35	MPFITEXY	8.46 ± 0.08	1.05 ± 0.11	0.34
Dynamical masses	35	LINMIX_ERR	8.46 ± 0.09	1.05 ± 0.12	0.36 ± 0.08
Stellar masses	18	MPFITEXY	8.56 ± 0.10	1.34 ± 0.15	0.17
Power law	12	MPFITEXY	8.43 ± 0.20	0.94 ± 0.39	0.50
Core	20	MPFITEXY	8.45 ± 0.15	1.09 ± 0.20	0.28
$L \leqslant 10^{10.8}\,L_\odot$	19	LINMIX_ERR	8.44 ± 0.14	1.05 ± 0.26	0.45 ± 0.13
$L > 10^{10.8}\,L_\odot$	12	LINMIX_ERR	7.66 ± 1.60	1.92 ± 1.72	0.38 ± 0.19
$L > 10^{10.8}\,L_\odot$	12	MPFITEXY	6.92 ± 1.05	2.72 ± 1.12	N/A
$M_{\rm bulge} \leqslant 10^{11.5}\,M_\odot$	21	LINMIX_ERR	8.54 ± 0.15	1.11 ± 0.28	0.47 ± 0.12
$M_{\rm bulge} > 10^{11.5}\,M_\odot$	14	LINMIX_ERR	7.28 ± 1.19	2.26 ± 1.33	0.30 ± 0.17
$M_{\rm bulge} > 10^{11.5}\,M_\odot$	14	MPFITEXY	7.03 ± 0.78	2.53 ± 0.85	N/A

Notes. For the $M_\bullet$–σ relation, we fit $\log_{10}(M_\bullet) = \alpha + \beta \log_{10}(\sigma/200\,{\rm km\,s^{-1}})$. Subsamples designated (0–$r_{\rm eff}$) define σ using kinematic data over the interval $0 < r < r_{\rm eff}$. For all other subsamples, we define σ using data over the interval $r_{\rm inf} < r < r_{\rm eff}$. For the $M_\bullet$–L relation, we fit $\log_{10}(M_\bullet) = \alpha + \beta \log_{10}(L/10^{11}\,L_\odot)$. Luminosities are in V band. For the $M_\bullet$–$M_{\rm bulge}$ relation, we fit $\log_{10}(M_\bullet) = \alpha + \beta \log_{10}(M_{\rm bulge}/10^{11}\,M_\odot)$. All fits except for the "stellar masses" line use the sample of bulges with dynamical masses.

Table 3
Galaxies with Dynamical Measurements of $M_\bullet$

Galaxy	$M_\bullet$ (+, −) ($M_\odot$)	Ref.	σ (km s^{-1})	log L_V	$M_{\rm bulge}$ ($M_\odot$)	Ref.	$r_{\rm inf}$ (″)	Morph.	D (Mpc)	Method
Milky Way[a]	4.1 (0.6,0.6) e6	1,2	103 ± 20				43	S	0.008	stars
A1836-BCG	3.9 (0.4,0.6) e9	3	288 ± 14	11.26 ± 0.06			0.27	E (C)	157.5	gas
A3565-BCG	1.4 (0.3,0.2) e9	3	322 ± 16	11.24 ± 0.06			0.22	E (C)	54.4	gas
Circinus	1.7 (0.4,0.3) e6	4	158 ± 18				0.02	S	4.0	masers
IC 1459[b]	2.8 (1.1,1.2) e9	5	315 ± 16	10.96 ± 0.06	3.07e11	45	0.81	E (C)	30.9	stars
N221 (M32)[y]	2.6 (0.5,0.5) e6	6	75 ± 3	8.52 ± 0.02	7.62e8	45	0.57	E (I)	0.73	stars
N224 (M31)[y]	1.4 (0.8,0.3) e8	7	160 ± 8				6.5	S	0.73	stars
N524[w]	8.6 (1.0,0.4) e8	8	235 ± 12	10.62 ± 0.04			0.57	S0 (C)	24.2	stars
N821[w]	1.7 (0.7,0.7) e8	9	209 ± 10	10.36 ± 0.05	1.92e11	9	0.14	E (I)	23.4	stars
N1023[w]	4.0 (0.4,0.4) e7	10	205 ± 10	10.06 ± 0.11	6.49e10	45	0.08	S0 (pl)	10.5	stars
N1194[c]	6.8 (0.3,0.3) e7	11	148^{+26}_{-22}				0.05	S0	55.5	masers
N1300	7.1 (3.4,1.8) e7	12	218 ± 10				0.07	S	20.1	gas
N1316[x]	1.7 (0.3,0.3) e8	13	226 ± 11	11.18 ± 0.05			0.14	E (I)	21.0	stars
N1332[w]	1.5 (0.2,0.2) e9	14	328 ± 16	10.16 ± 0.05			0.54	S0 (pl)	22.7	stars
N1374[b,x]	5.9 (0.6,0.5) e8	15	174 ± 9	10.10 ± 0.05	5.79e10	15	0.89	E (C)	19.6	stars
N1399[b,d,x]	5.1 (0.6,0.7) e8	16	296 ± 15	10.78 ± 0.04	3.98e11	46	0.25	E (C)	20.9	stars
N1399[b,d,x]	1.3 (0.5,0.7) e9	17	296 ± 15	10.78 ± 0.04	3.98e11	46	0.63	E (C)	20.9	stars
N1407[b,w]	4.7 (0.7,0.5) e9	15	274 ± 14	11.05 ± 0.05	1.00e12	15	1.9	E (C)	29.0	stars
N1550[b]	3.9 (0.7,0.7) e9	15	289 ± 14	10.87 ± 0.05			0.78	E (I)	53.0	stars
N2273[c]	7.8 (0.4,0.4) e6	11	144^{+18}_{-15}				0.01	S	26.8	masers
N2549[w]	1.4 (0.1,0.4) e7	8	145 ± 7	9.55 ± 0.04	1.99e10	8	0.05	S0 (pl)	12.7	stars
N2787[w]	4.1 (0.4,0.5) e7	18	189 ± 9				0.14	S0 (pl)	7.5	gas
N2960[c]	1.21 (0.05,0.05) e7	11	166^{+16}_{-15}				0.01	S	75.3	masers
N3031 (M81)	8.0 (2.0,1.1) e7	19	143 ± 7				0.85	S	4.1	gas
N3091	3.7 (0.1,0.5) e9	15	307 ± 15	11.00 ± 0.05			0.66	E (C)	52.7	stars
N3115[w]	8.9 (5.1,2.7) e8	20	230 ± 11	10.34 ± 0.02	1.57e11	45	1.6	S0 (pl)	9.5	stars
N3227	1.5 (0.5,0.8) e7	21	133 ± 12				0.04	S	17.0	stars
N3245[w]	2.1 (0.5,0.6) e8	22	205 ± 10		7.00e10	45	0.21	S0 (pl)	21.5	gas
N3368[w]	7.6 (1.6,1.5) e6	23	122^{+28}_{-24}				0.04	S	10.6	stars
N3377[w]	1.8 (0.9,0.9) e8	9	145 ± 7	9.93 ± 0.04	2.35e10	9	0.69	E (pl)	11.0	stars
N3379 (M105)[w]	4.2 (1.0,1.1) e8	24	206 ± 10	10.29 ± 0.01	6.86e10	45	0.83	E (C)	10.7	stars
N3384[w]	1.1 (0.5,0.5) e7	9	143 ± 7	9.89 ± 0.09	1.90e10	9	0.04	S0 (pl)	11.5	stars
N3393	3.3 (0.2,0.2) e7	25	148 ± 10				0.03	S	53.6	masers
N3489[w]	6.0 (0.8,0.9) e6	23	100^{+15}_{-11}				0.04	S0	12.0	stars
N3585[w]	3.3 (1.5,0.6) e8	26	213 ± 10	10.66 ± 0.08	1.60e11	26	0.31	S0 (I)	20.6	stars
N3607[e,w]	1.4 (0.4,0.5) e8	26	229 ± 11				0.10	E (C)	22.6	stars
N3608[w]	4.7 (1.0,1.0) e8	9	182 ± 9	10.34 ± 0.04	7.66e10	9	0.55	E (C)	22.8	stars
N3842[b]	9.7 (3.0,2.5) e9	27	270 ± 14	11.20 ± 0.05	1.55e12	44	1.2	E (C)	98.4	stars
N3998[b,w]	8.5 (0.7,0.7) e8	28	272 ± 14	9.91 ± 0.04			0.71	S0 (pl)	14.3	stars
N4026[w]	1.8 (0.6,0.3) e8	26	180 ± 9	9.73 ± 0.08	2.81e10	26	0.37	S0 (pl)	13.4	stars
N4258[w]	3.67 (0.01,0.01) e7	29	115 ± 10				0.35	S	7.0	masers
N4261[w]	5.3 (1.1,1.1) e8	30	315 ± 15	11.00 ± 0.02	8.26e11	45	0.15	E (C)	32.6	gas
N4291[w]	9.8 (3.1,3.1) e8	9	242 ± 12	10.25 ± 0.05	9.96e10	9	0.56	E (C)	26.6	stars
N4342[z]	4.6 (2.6,1.5) e8	31	225 ± 11		1.80e10	45	0.35	S0 (pl)	23.0	stars
N4374 (M84)[x]	9.2 (1.0,0.8) e8	32	296 ± 14	10.98 ± 0.02	3.62e11	45	0.51	E (C)	18.5	gas
N4388[c]	8.8 (0.2,0.2) e6	11	107^{+8}_{-7}				0.03	S	19.8	masers
N4459[x]	7.0 (1.3,1.4) e7	18	167 ± 8	10.31 ± 0.02			0.14	E (pl)	16.0	gas
N4472 (M49)[x]	2.5 (0.6,0.1) e9	15	300 ± 15	11.05 ± 0.05	8.98e11	15	1.3	E (C)	16.7	stars
N4473[x]	8.9 (4.5,4.4) e7	9	190 ± 9	10.29 ± 0.02	1.61e11	9	0.15	E (C)	15.2	stars
N4486 (M87)[b,x]	6.2 (0.3,0.4) e9	33	324^{+28}_{-16}	11.08 ± 0.02	1.31e12	47	3.1	E (C)	16.7	stars
N4486A[x]	1.4 (0.5,0.5) e7	34	111 ± 5	9.48 ± 0.02			0.06	E (pl)	18.4	stars
N4564[f,x]	8.8 (2.4,2.4) e7	9	162 ± 8		4.66e10	45	0.19	S0 (pl)	15.9	stars
N4594 (M104)[b,w]	6.7 (0.5,0.4) e8	35	230 ± 12				1.1	S	10.0	stars
N4596	8.4 (3.6,2.5) e7	18	136 ± 6				0.22	S0 (pl)	18.0	gas
N4649 (M60)[b,x]	4.7 (1.1,1.0) e9	36	341 ± 17	10.99 ± 0.02	7.72e11	36	2.2	E (C)	16.5	stars
N4697[x]	2.0 (0.2,0.2) e8	9	177 ± 8	10.46 ± 0.04	1.29e11	9	0.46	E (pl)	12.5	stars
N4736 (M94)[g,w]	6.8 (1.6,1.6) e6	37	112 ± 6				0.10	S	5.0	stars
N4826 (M64)[g,w]	1.6 (0.4,0.4) e6	37	96 ± 5				0.02	S	7.3	stars
N4889[b]	2.1 (1.6,1.55) e10	27	347 ± 17	11.48 ± 0.05	1.75e12	46	1.5	E (C)	103.2	stars
N5077	8.0 (5.0,3.3) e8	38	222 ± 11	10.75 ± 0.05	3.66e11	38	0.32	E (C)	44.9	gas
N5128 (Cen A)[h,w]	5.9 (1.1,1.0) e7	39	150 ± 7	10.60 ± 0.03			0.60	S0/E (C)	4.1	stars
N5516	4.0 (0.1,1.1) e9	15	306 ± 26	11.22 ± 0.05			0.63	E (C)	60.1	stars
N5576[w]	1.7 (0.3,0.4) e8	26	183 ± 9	10.39 ± 0.05	9.58e10	26	0.18	E (C)	25.7	stars
N5845[w]	4.9 (1.5,1.6) e8	9	234 ± 11	9.75 ± 0.05	3.36e10	9	0.31	E (pl)	25.9	stars
N6086	3.8 (1.7,1.2) e9	40	318 ± 16	11.23 ± 0.05	1.43e12	40	0.24	E (C)	139.1	stars

Table 3
(Continued)

Galaxy	$M_\bullet$ (+, −) ($M_\odot$)	Ref.	σ (km s^{-1})	log L_V	$M_{\rm bulge}$ ($M_\odot$)	Ref.	$r_{\rm inf}$ ($''$)	Morph.	D (Mpc)	Method
N6251	6.0 (2.0,2.0) e8	41	290 ± 14		5.60e11	46	0.06	E (pl)	106.0	gas
N6264[c]	3.03 (0.05,0.04) e7	11	158^{+16}_{-14}				0.01	S	145.4	masers
N6323[c]	9.8 (0.1,0.1) e6	11	158^{+28}_{-23}				0.003	S	110.5	masers
N7052	4.0 (2.8,1.6) e8	42	266 ± 13	10.92 ± 0.04	3.50e11	45	0.07	E (C)	70.9	gas
N7582	5.5 (1.6,1.1) e7	43	156 ± 19				0.09	S	22.3	gas
N7619[b,w]	2.3 (1.2,0.1) e9	15	313 ± 16	11.07 ± 0.05			0.39	E (C)	53.9	stars
N7768[b]	1.3 (0.5,0.4) e9	44	257 ± 13	11.09 ± 0.05	1.16e12	44	0.14	E (C)	112.8	stars
U3789[c]	1.08 (0.06,0.05) e7	11	107^{+13}_{-12}				0.02	S	48.4	masers

Notes. The first reference column corresponds to the black hole mass measurement, and the second corresponds to the measurement of $M_\star/L$ used to compute $M_{\rm bulge}$. Bulge luminosity L_V is in solar units. Quoted errors (+, −) for $M_\bullet$ are 68% confidence intervals. We assume 0.24 dex uncertainty for all $M_{\rm bulge}$ values. The black hole radius of influence $r_{\rm inf}$ is defined by $GM_\bullet/\sigma^2$. Morphologies include designations for power law (pl), core (C), and intermediate (I) surface brightness profiles. Distances for 44 objects have been updated since the compilation of McConnell et al. (2011a); see notes w–z below. A more detailed version of this table is available at http://blackhole.berkeley.edu. Notes on individual galaxies:

[a] The literature contains a large number of estimates for the velocity dispersion of our Galaxy's bulge, using different kinematic tracers at different radii. We use the radially averaged measurement of $\sigma = 103 \pm 20$ km s^{-1} from Tremaine et al. (2002).

[b] We have re-computed σ for 12 galaxies, considering kinematic data between $r_{\rm inf}$ and $r_{\rm eff}$. The corresponding values of σ are listed here. Table 1 also lists the values of σ using data from 0 to $r_{\rm eff}$.

[c] Maser-based black hole masses for several galaxies are presented in Greene et al. (2010) and Kuo et al. (2011). We use the velocity dispersions presented in Greene et al. (2010). For consistency with the rest of our sample, we use the black hole masses from Kuo et al. (2011), which agree with the values in Greene et al. (2010) but do not include distance uncertainties in the overall uncertainty for $M_\bullet$. Braatz et al. (2010) provide an updated distance and black hole mass for UGC 3789, which are consistent with the values we adopt from Kuo et al. (2011).

[d] Following G09, our sample includes two distinct measurements for NGC 1399. We weight each of these measurements by 50% when performing fits to the black hole scaling relations.

[e] The literature contains two inconsistent estimates of the V-band luminosity of NGC 3607: $M_V = -21.62$ in G09, and $M_V = -19.88$ in Lauer et al. (2007a).

[f] The literature contains two inconsistent estimates of the V-band bulge luminosity of NGC 4564: $M_V = -19.60$ in G09, and $M_V = -20.26$ in Lauer et al. (2007a).

[g] Bulge luminosities for NGC 4736 and NGC 4826 were included in the sample of McConnell et al. (2011a) and their fit to the $M_\bullet$–L relation. These luminosities corresponded to pseudobulges identified in Kormendy et al. (2011), and we have not included them in our present fits.

[h] The stellar dynamical measurement of $M_\bullet$ in NGC 5128 by Cappellari et al. (2009) is fully consistent with the molecular gas measurement $M_\bullet = 5.3^{+0.6}_{-0.4}\,M_\odot$ by Neumayer et al. (2007).

[w] We have updated the distances to 29 galaxies using surface brightness fluctuation measurements from Tonry et al. (2001), with the corrections suggested by Blakeslee et al. (2010).

[x] We have updated the distances to 12 galaxies using surface brightness fluctuation measurements from Blakeslee et al. (2009), which are based on data from ACS on the *Hubble Space Telescope*.

[y] We have adopted a distance of 0.73 Mpc to M31, based on Cepheid variable measurements by Vilardell et al. (2007). We assume that M31 and M32 lie at the same distance.

[z] For NGC 4342, we have adopted the distance of 23 Mpc by Bogdán et al. (2012).

References. (1) Ghez et al. 2008; (2) Gillessen et al. 2009; (3) Dalla Bontà et al. 2009; (4) Greenhill et al. 2003; (5) Cappellari et al. 2002; (6) Verolme et al. 2002; (7) Bender et al. 2005; (8) Krajnović et al. 2009; (9) Schulze & Gebhardt 2011; (10) Bower et al. 2001; (11) Kuo et al. 2011; (12) Atkinson et al. 2005; (13) Nowak et al. 2008; (14) Rusli et al. 2011; (15) Rusli 2012; (16) Gebhardt et al. 2007; (17) Houghton et al. 2006; (18) Sarzi et al. 2001; (19) Devereux et al. 2003; (20) Emsellem et al. 1999; (21) Davies et al. 2006; (22) Barth et al. 2001; (23) Nowak et al. 2010; (24) van den Bosch & de Zeeuw 2010; (25) Kondratko et al. 2008; (26) Gültekin et al. 2009b; (27) McConnell et al. 2011a; (28) Walsh et al. 2012; (29) Herrnstein et al. 2005; (30) Ferrarese et al. 1996; (31) Cretton & van den Bosch 1999; (32) Walsh et al. 2010; (33) Gebhardt et al. 2011; (34) Nowak et al. 2007; (35) Jardel et al. 2011; (36) Shen & Gebhardt 2010; (37) Kormendy et al. 2011; (38) de Francesco et al. 2008; (39) Cappellari et al. 2009; (40) McConnell et al. 2011b; (41) Ferrarese & Ford 1999; (42) van der Marel & van den Bosch 1998; (43) Wold et al. 2006; (44) McConnell et al. 2012; (45) Häring & Rix 2004; (46) Magorrian et al. 1998; (47) Gebhardt & Thomas 2009.

the effect of decreasing σ and increasing the slope of the $M_\bullet$–σ relation. We have obtained new values of σ for 12 galaxies in our sample by examining kinematic profiles from the literature and excluding data within $r_{\rm inf}$; these galaxies are listed in Table 1. Ten of the twelve galaxies have $\sigma > 250$ km s^{-1} using either definition.

In Table 2 we test how much the definition of σ affects our fit to our full sample of 72 galaxies, as well as subsamples dominated by massive early-type galaxies (see rows labeled "0–$r_{\rm eff}$"). We find the slope of the global $M_\bullet$–σ relation to change slightly from $\beta = 5.64 \pm 0.32$ in our fiducial sample (in which $\sigma(r_{\rm inf}$–$r_{\rm eff})$ is used) to $\beta = 5.48 \pm 0.30$ for the conventional definition of σ with $r_{\rm min} = 0$ in Equation (1). The latter is a fairer quantity to be compared with earlier studies, but the resulting $M_\bullet$–σ relation is still significantly steeper than those reported in G09 and B12. The definition of σ does not significantly affect our measurements of the intrinsic scatter in $\log(M_\bullet)$ (see Table 2 and Section 4).

3.2.5. *High versus Low σ*

To search for possible systematic deviations of the $M_\bullet$–σ relation from a single power law, we divide the galaxies into low-σ and high-σ subsamples, separated by a cutoff value $\sigma_{\rm cut}$. We have tested numerous values of $\sigma_{\rm cut}$ in search of robust trends. Our strongest finding is that the relation for the higher-σ sample appears to steepen drastically when $\sigma_{\rm cut} \gtrsim 270$ km s^{-1}. As shown in Table 2 (for $\sigma_{\rm cut} = 275$ km s^{-1}), the `MPFITEXY` and `LINMIX_ERR` procedures both return nearly vertical relations, with very large uncertainties in β. This suggests a breakdown of the $M_\bullet$–σ correlation as the galaxy population "saturates" at $\sigma \sim 350$ km s^{-1}. Saturation of the L–σ and $M_\bullet$–σ relations has been predicted from observations and simulations of the most

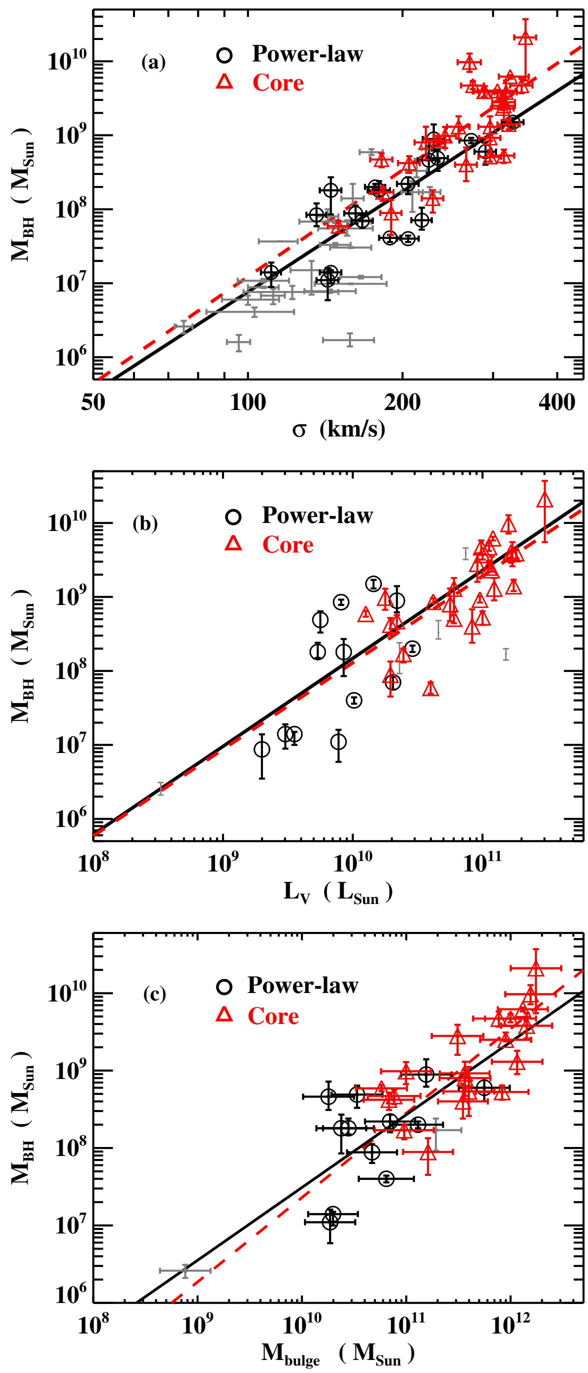

Figure 4. Black hole scaling relations, with separate fits for power-law galaxies (solid black lines), vs. core galaxies (dashed red lines). (a) $M_\bullet$–σ relation. (b) $M_\bullet$–L relation. (c) $M_\bullet$–$M_{\rm bulge}$ relation.

(A color version of this figure is available in the online journal.)

massive galaxies (e.g., Boylan-Kolchin et al. 2006; Bernardi et al. 2007; Lauer et al. 2007a). The MPFITEXY procedure returns zero intrinsic scatter when fitting galaxies with $\sigma > 275$ km s^{-1}; this is an artifact of the large slope.

One might suspect that the saturation in $M_\bullet(\sigma)$ results from the lower σ values we obtained for 12 galaxies after excluding data within $r_{\rm inf}$. We have also fit the high-σ and low-σ subsamples using the conventional definition of σ. We still find that the highest-σ galaxies follow a very steep $M_\bullet$–σ relation, although this trend begins to appear at slightly higher values of $\sigma_{\rm cut}$ (exemplified by $\sigma_{\rm cut} = 290$ km s^{-1} in Table 2).

A weaker trend occurs for $\sigma_{\rm cut}$ in the range 175–225 km s^{-1}. Here, the higher-σ sample exhibits a steeper slope ($\beta \sim$ 6–7) than the lower-σ sample ($\beta \sim 5$). Still, the differences between the fits for the two subsamples are within 1σ error bars as the uncertainties in α and β are large. This trend vanishes when we adopt the conventional definition of σ (data from $r =$ 0 to $r_{\rm eff}$). As an example, Table 2 lists the fitting results for $\sigma_{\rm cut} = 200$ km s^{-1}.

It is tempting to fit $M_\bullet(\sigma)$ for narrow intervals in σ (e.g., 150 km s^{-1} $< \sigma <$ 200 km s^{-1}), but the intrinsic scatter in the $M_\bullet$–σ relation drives these samples toward an uncorrelated distribution. For the current sample of $M_\bullet$, a long baseline in σ ($\gtrsim$100 km s^{-1}) is therefore needed to determine the slope of the $M_\bullet$–σ relation.

We have also tried fitting $M_\bullet(\sigma)$ for subsamples defined by cuts in L and $M_{\rm bulge}$; two examples are listed in Table 2. Some of the high-L subsamples exhibit a steep $M_\bullet$–σ slope, but again with large uncertainties.

3.2.6. A Log-quadratic Fit to $M_\bullet$–σ

In light of evidence that the $M_\bullet$–σ relation steepens toward high galaxy masses, we have also attempted to fit $M_\bullet(\sigma)$ as a log-quadratic function in Equation (3). The coefficients α, β, β_2, and intrinsic scatter ϵ_0 for our 72-galaxy sample are determined from a brute-force least-squares estimator similar to MPFITEXY. We find that the best-fit parameters are $\alpha = 8.28 \pm 0.07$, $\beta =$ 5.76 ± 0.34, $\beta_2 = 1.68 \pm 1.82$, and $\epsilon_0 = 0.38$. Uncertainties in α, β, and β_2 are determined by assessing the one-dimensional likelihood function after marginalizing χ^2 with respect to the other two parameters. We find $\beta_2 > 0$ with 82% confidence, slightly below the 1σ threshold for a one-sided confidence interval.

As suggested by the highly uncertain power-law slopes for high-σ galaxies, our measurement of upward curvature in $M_\bullet(\sigma)$ is marginal. Adopting a quadratic relation does not decrease the intrinsic scatter in $M_\bullet$. Our full sample updates the investigations of Wyithe (2006a, 2006b; 31 galaxies) and G09 (49 galaxies), who reported similar confidence levels for a non-zero quadratic term. At the extreme end of the local galaxy velocity dispersion function ($\sigma \sim 400$ km s^{-1}), our best quadratic fit predicts black hole masses ∼40% higher than the best power-law fit.

3.3. $M_\bullet$–L and $M_\bullet$–M_{bulge} Relations

In Table 3, we present V-band luminosities for 44 galaxies and dynamically measured bulge masses for 35 galaxies. For several of the late-type galaxies in our sample, the literature contains one or more estimates of the bulge-to-total light ratio. Rather than judging between the various estimates, we present results for the early types only. Our best fit values are $\beta = 1.11 \pm 0.13$ and $\alpha = 9.23 \pm 0.10$ for the $M_\bullet$–L relation, and $\beta = 1.05 \pm 0.11$ and $\alpha = 8.46 \pm 0.08$ for the $M_\bullet$–$M_{\rm bulge}$ relation.

Additional fits to subsamples of these galaxies are listed in Table 2. The $M_\bullet$–L and $M_\bullet$–$M_{\rm bulge}$ relations do not show statistically significant differences between core and power-law galaxies (see also Figures 4(b) and (c)).

Figures 2 and 3 show that our $M_\bullet$–L and $M_\bullet$–$M_{\rm bulge}$ samples both appear to have a central knot, where black holes with $10^8\,M_\odot < M_\bullet < 10^9\,M_\odot$ exhibit relatively weak correlation with L or $M_{\rm bulge}$. This feature makes it difficult to interpret the fits to high-L and low-L (or high-$M_{\rm bulge}$ and low-$M_{\rm bulge}$) subsamples. We find tentative evidence that the most luminous and massive galaxies ($L > 10^{10.8}\,L_\odot$; $M_{\rm bulge} > 10^{11.5}\,M_\odot$)

have steeper slopes in $M_\bullet(L)$ and $M_\bullet(M_{\rm bulge})$, as exemplified in Table 2. Both samples are sparsely populated at the low-$M_\bullet$ end.

3.4. Comparison to Previous Studies

The slope of the $M_\bullet$–σ relation reported in prior studies has wavered between ∼4 (e.g., Gebhardt et al. 2000; Tremaine et al. 2002; G09; B12) and ∼5 (e.g., Ferrarese & Merritt 2000; Merritt & Ferrarese 2001; Graham et al. 2011). Our best-fit slope for the global $M_\bullet$–σ relation falls at the steep end of this distribution, while various subsamples exhibit a wider range of slopes ($\beta \approx 3.8$ to $\beta > 12$). In particular, the $M_\bullet$–σ relation for our full sample is significantly steeper than those reported in G09 ($\beta = 4.24 \pm 0.41$) and B12 ($\beta = 4.42 \pm 0.30$). This steepening has occurred because the newest measurements of $M_\bullet$ in early-type galaxies (higher σ) mostly fall above the global $M_\bullet$–σ relation, and the newest measurements of $M_\bullet$ in late-type galaxies (lower σ) mostly fall below the global relation. In addition to the significant discrepancy between the two subsamples' best-fit intercepts, both the early- and late-type $M_\bullet$–σ relations have steepened.

Our fit to early-type galaxies is significantly steeper than the early-type fit by G09 ($\beta = 5.20 \pm 0.36$, versus $\beta = 3.96 \pm 0.42$). This difference is largely due to several updates to the high-σ galaxy sample: new measurements of $M_\bullet \sim 10^{10}\,M_\odot$ in the brightest cluster galaxies NGC 4889 and NGC 3842 (McConnell et al. 2011a), new measurements of $M_\bullet > 10^9\,M_\odot$ in seven more galaxies (Rusli et al. 2011; Rusli 2012), and updated measurements increasing $M_\bullet$ in M87 and M60 (Gebhardt & Thomas 2009; Shen & Gebhardt 2010). Defining σ to exclude the black hole radius of influence further steepens the early-type galaxy sample by a small amount. If we exclude the recent additions by McConnell et al. (2011a, 2011b, 2012) and Rusli (2012), we obtain $\beta = 4.77 \pm 0.36$ for 42 early-type galaxies. Removing M87 and M60 further reduces β to 4.55 ± 0.37; in addition to revised black hole masses, these two galaxies exhibit some of the largest differences in σ in Table 1.

Our fit for late-type galaxies is slightly steeper than G09 ($\beta = 5.06 \pm 1.16$, versus $\beta = 4.58 \pm 1.58$). This arises primarily from our exclusion of NGC 1068 and NGC 2748.

Our earlier compilation of a similar sample of 67 galaxies (McConnell et al. 2011a) gave $\alpha = 8.28 \pm 0.06$ and $\beta = 5.13 \pm 0.34$ for the $M_\bullet$–σ relation. Our $M_\bullet(\sigma)$ fit to the present sample of 72 galaxies has a steeper slope of 5.64 ± 0.32, largely due to the exclusion of NGC 7457, which had the lowest velocity dispersion ($\sigma = 67\,{\rm km\,s^{-1}}$) of all galaxies in the previous sample (see Section 2 and Gebhardt et al. 2003 for discussion of this galaxy's central massive object). If we include NGC 7457 in our present sample, we obtain $\alpha = 8.33 \pm 0.05$, $\beta = 5.42 \pm 0.31$, and $\epsilon_0 = 0.40$, closer to our earlier results.

Our $M_\bullet$–L and $M_\bullet$–$M_{\rm bulge}$ slopes are consistent with a number of previous investigations, including multiple bandpasses for L (e.g., Marconi & Hunt 2003; Häring & Rix 2004; McLure & Dunlop 2004; G09; Schulze & Gebhardt 2011). For the $M_\bullet$–L relation, Sani et al. (2011) report different $M_\bullet$–$L_{3.6\,\mu{\rm m}}$ and $M_\bullet$–L_V slopes and suggest that color corrections and extinction may be responsible for the difference. Their $M_\bullet$–$L_{3.6\,\mu{\rm m}}$ slope is 0.93 ± 0.10, while their $M_\bullet$–L_V slope ranges from 1.11 to 1.40 depending on the regression method. These slopes are consistent with our $M_\bullet$–L_V slope of 1.11 ± 0.13.

For the $M_\bullet$–$M_{\rm bulge}$ relation, the latest compilation of 46 galaxies by B12 gives a slope of 0.79 ± 0.26. We note that their $M_{\rm bulge}$ values are virial estimates based on the galaxies' σ and $r_{\rm eff}$ via $M_{\rm bulge} = 5.0\sigma^2 r_{\rm eff}/G$. In comparison, our $M_{\rm bulge}$ values use the mass-to-light ratios obtained from dynamical models.

Recently, Graham (2012) examined the $M_\bullet$–σ and $M_\bullet$–$M_{\rm bulge}$ relations with separate fits to core and non-core galaxies, based on the galaxy sample of Häring & Rix (2004) and updated black hole masses from Graham et al. (2011). The non-core galaxies were found to follow a very steep $M_\bullet$–$M_{\rm bulge}$ relation ($\beta \sim 2$), and there was virtually no difference in the $M_\bullet$–σ relations for core versus non-core galaxies. Our relative trends for core and power-law galaxies differ from those in Graham (2012). This is likely due to differences in the galaxy samples: our core galaxies include 11 galaxies with $M_\bullet > 10^9\,M_\odot$ that are absent from the sample used by Graham (2012). Our photometric classification of galaxies also differs from Graham (2012). In particular, we classify the high-$M_{\rm bulge}$ object NGC 6251 as a power-law galaxy, based on the surface brightness profile of Ferrarese & Ford (1999). Excluding NGC 6251, we measure $\beta \approx 1.6$ for power-law galaxies on the $M_\bullet$–$M_{\rm bulge}$ relation.

4. SCATTER IN BLACK HOLE MASS

For a given black hole scaling relation, the differences between the measured values of $M_\bullet$ and the mean power-law relation are conventionally interpreted as a combination of measurement errors and intrinsic scatter. We assume the scatter in $M_\bullet$ to be lognormal, and define the intrinsic scatter term ϵ_0 such that

$$\chi^2 = \sum_i \frac{[\log_{10}(M_{\bullet,i}) - \alpha - \beta x_i]^2}{\epsilon_0^2 + \epsilon_{M,i}^2 + \beta^2 \epsilon_{x,i}^2} \;, \tag{4}$$

where $x = \log_{10}(\sigma/200\,{\rm km\,s^{-1}})$ for the $M_\bullet$–σ relation, $x = \log_{10}(L/10^{11}\,L_\odot)$ for the $M_\bullet$–L relation, and $x = \log_{10}(M_{\rm bulge}/10^{11}\,M_\odot)$ for the $M_\bullet$–$M_{\rm bulge}$ relation. Here, ϵ_M is the 1σ error in $\log_{10}(M_\bullet)$, and ϵ_x is the 1σ error in x. For a given sample and power-law fit, we adopt the value of ϵ_0 for which $\chi^2_\nu = 1$ ($\chi^2 = N_{\rm dof}$). G09 tested several forms of intrinsic scatter in $M_\bullet$ and found lognormal scatter to be an appropriate description.

Fitting the full galaxy sample for each scaling relation, we find the intrinsic scatter in $\log_{10}(M_\bullet)$ to be $\epsilon_0 = 0.38$ for the $M_\bullet$–σ relation, $\epsilon_0 = 0.49$ for the $M_\bullet$–L relation, and $\epsilon_0 = 0.34$ for the $M_\bullet$–$M_{\rm bulge}$ relation (or $\epsilon_0 = 0.17$ for $M_\bullet$ versus stellar $M_{\rm bulge}$). While it is tempting to conclude that $M_{\rm bulge}$ is the superior predictor of $M_\bullet$, the relative errors in $M_{\rm bulge}$, σ, and L demand a more cautious interpretation. As noted in Section 2, we have assumed that all $M_{\rm bulge}$ values have an error of at least 0.24 dex. We have repeated our fits to $M_\bullet(M_{\rm bulge})$ with a minimum error of only 0.09 dex. Fitting the full $M_{\rm bulge}$ sample with this reduced error in $M_{\rm bulge}$, we obtain a larger intrinsic scatter ($\epsilon_0 = 0.39$) as expected from Equation (4), while the slope and intercept of the fit do not change significantly. Similarly, our measurements of ϵ_0 for the $M_\bullet$–σ and $M_\bullet$–L relations depend in part upon the assumed errors in σ ($\geqslant 5\%$, following G09) and L (typically <0.05 dex). In addition to evaluating ϵ_0, Novak et al. (2006) used earlier data sets to assess which correlation yielded the lowest predictive uncertainty in $M_\bullet$, given a set of host galaxy properties with measurement errors. They found the $M_\bullet$–σ relation to be marginally favorable for predicting black holes with $M_\bullet \sim 10^8\,M_\odot$, but noted that uncertainties in the relations' slopes complicated predictions near the extrema of the relations. Our global $M_\bullet$–σ relation has a steeper slope ($\beta = 5.64$) than the samples evaluated by Novak et al. (2006), with β from 3.69 to 4.59.

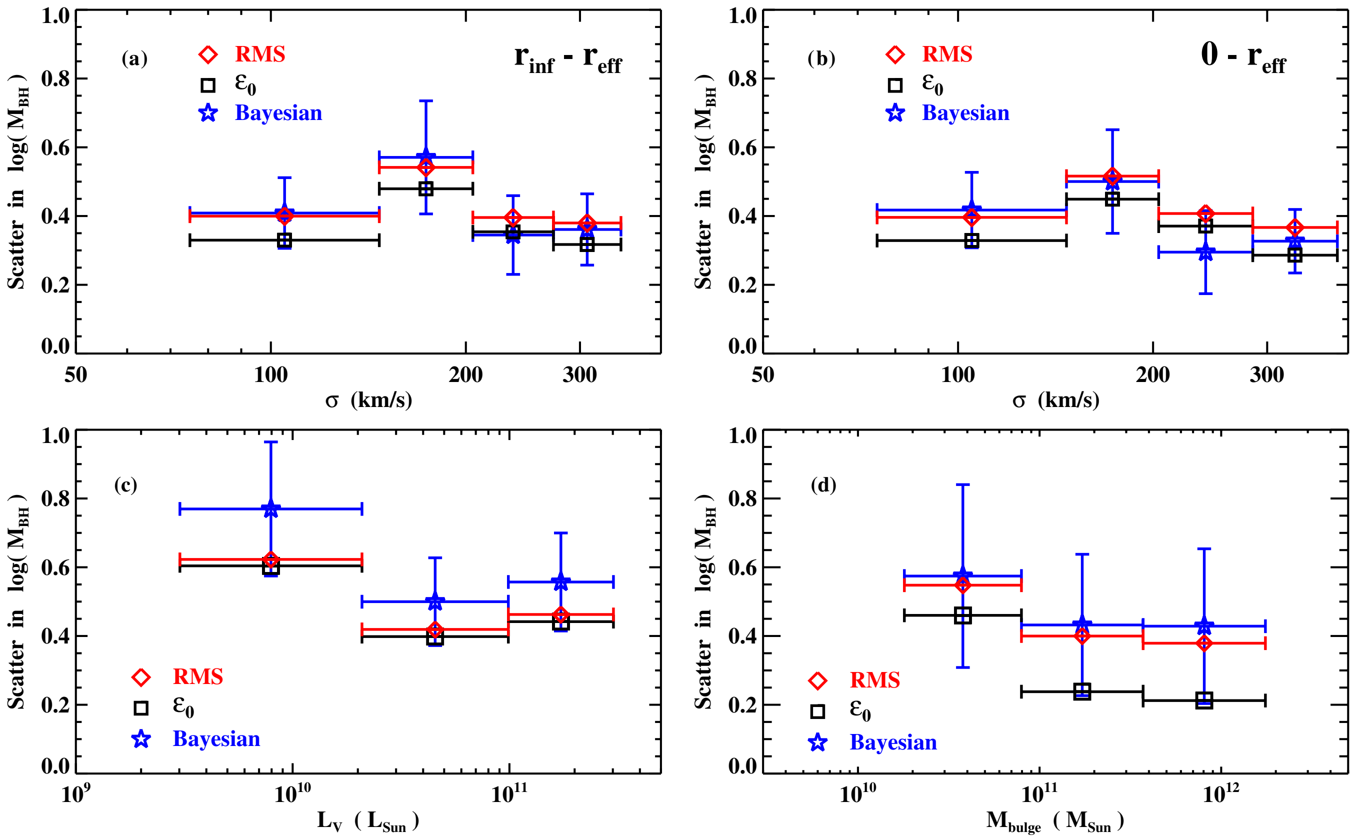

Figure 5. Scatter in $\log_{10} M_\bullet$ for different intervals in σ, L, and $M_{\rm bulge}$. Black squares represent the intrinsic scatter ϵ_0 required to obtain $\chi^2 = N_{\rm gal}$ between the subsample of galaxies and the global scaling relation. Red diamonds represent the rms residual for each interval, between $\log(M_\bullet)$ and the global scaling relation. Blue stars with vertical error bars represent the Bayesian estimates for ϵ_0, obtained while fitting a separate scaling relation for each interval. (a) Scatter with respect to the $M_\bullet$–σ relation, $\log_{10} M_\bullet = 8.32 + 5.64 \log_{10}(\sigma/200\,{\rm km\,s^{-1}})$, defining σ with data from $r_{\rm inf}$ to $r_{\rm eff}$. (b) Scatter with respect to the $M_\bullet$–σ relation, $\log_{10} M_\bullet = 8.29 + 5.48 \log_{10}(\sigma/200\,{\rm km\,s^{-1}})$, defining σ with data from 0 to $r_{\rm eff}$. (c) Scatter with respect to the $M_\bullet$–L relation, $\log_{10} M_\bullet = 9.23 + 1.11 \log_{10}(L/10^{11}\,L_\odot)$. (d) Scatter with respect to the $M_\bullet$–$M_{\rm bulge}$ relation, $\log_{10} M_\bullet = 8.46 + 1.05 \log_{10}(M_{\rm bulge}/10^{11}\,M_\odot)$.

(A color version of this figure is available in the online journal.)

Beyond the intrinsic scatter ϵ_0 in black hole mass for the full sample, the dependence of ϵ_0 on σ, L, and $M_{\rm bulge}$ is a useful quantity for constraining theoretical models of black hole assembly. Successive mergers are predicted to drive galaxies toward the mean $M_\bullet$–$M_{\rm bulge}$ relation, especially when black hole growth is dominated by black hole–black hole mergers (e.g., Peng 2007; Jahnke & Macciò 2011). Understanding intrinsic scatter in $M_\bullet$ is also crucial for estimating the mass function of black holes, starting from the luminosity function or velocity dispersion function of galaxies (e.g., Lauer et al. 2007c; Tundo et al. 2007; G09).

Figure 5 illustrates how ϵ_0 varies across each of the $M_\bullet$–σ, $M_\bullet$–L, and $M_\bullet$–$M_{\rm bulge}$ relations for our updated sample of measurements. For each relation, we construct three or four bins containing equal numbers of galaxies and perform multiple estimates of the scatter in each bin. One estimate, represented by blue stars in Figure 5, is to perform an independent Bayesian fit (with `LINMIX_ERR`) for the scaling relation in each bin, and assess the posterior distribution of ϵ_0. This method provides uncertainties for ϵ_0 in each bin, but the fits to narrow data intervals typically yield poor estimates for the slope and intercept. A second estimate, represented by black squares in Figure 5, is to compute ϵ_0 as in Equation (4), using the global fit to the scaling relation to define the same values of α and β for all bins. The third and simplest estimate, represented by red diamonds in Figure 5, is to evaluate the root-mean-squared (rms) residual between $\log(M_\bullet)$ and the global scaling relation. The ϵ_0 term in Equation (4) provides a reliable assessment of intrinsic scatter only if random measurement errors are small: measurements with large uncertainties can yield $\chi^2_\nu \leqslant 1$ with no intrinsic scatter term. In comparison, the rms estimate has no explicit dependence on measurement errors.

Figures 5(a) and (b) illustrate the scatter in $M_\bullet$ as a function of σ. Two definitions of σ for the 12 galaxies in Table 1 are shown for comparison, where σ is computed from data between radii $r_{\rm inf}$ and $r_{\rm eff}$, or between 0 and $r_{\rm eff}$. Considering the large error bars in ϵ_0 from the Bayesian fits, we find no significant variation in $M_\bullet$ with respect to σ. The high- and low-mass ends of the $M_\bullet$–σ relation both exhibit ∼0.3–0.4 dex of scatter, regardless of how σ is defined or how scatter is estimated.

For the $M_\bullet$–L and $M_\bullet$–$M_{\rm bulge}$ relations, we find possible evidence that galaxies with low spheroid luminosities ($L < 10^{10.3}\,L_\odot$) and small stellar masses ($M_{\rm bulge} < 10^{11}\,M_\odot$) exhibit increased intrinsic scatter in $M_\bullet$. However, the scatter appears constant for galaxies above this range, spanning $10^{10.3}\,L_\odot < L < 10^{11.5}\,L_\odot$ and $10^{11}\,M_\odot < M_{\rm bulge} < 10^{12.3}\,M_\odot$. More measurements in the range $M_{\rm bulge} \sim 10^8$–$10^{10}\,M_\odot$ are needed to reveal whether intrinsic scatter in $M_\bullet$ varies systematically across an extended range of bulge luminosities or masses. The Bayesian estimates of ϵ_0 in each bin have large uncertainties; adopting this method, we do not detect a significant change in scatter for any interval in σ, L, or $M_{\rm bulge}$.

The Local Group galaxy M32 is separated from the other early-type galaxies in our sample by almost an order of magnitude in L, and more than an order of magnitude in $M_{\rm bulge}$. We have excluded its contribution in Figures 5(c) and (d), so that the sizes of the leftmost bins better reflect the sampled distributions of L and $M_{\rm bulge}$. Including M32 does not substantially change the amount of scatter in the lowest-L and lowest-$M_{\rm bulge}$ bins.

Although our three estimates of scatter do not yield the same absolute values, their qualitative trends as a function of σ, L, or $M_{\rm bulge}$ are very similar. The similar behavior of ϵ_0 and rms indicates that variations in measurement errors are not responsible for the apparent trends in intrinsic scatter.

5. SUMMARY AND DISCUSSION

We have compiled an updated sample of 72 black hole masses and host galaxy properties in Table 3; a more detailed version of Table 3 is available at http://blackhole.berkeley.edu. Compared with the 49 objects in G09, 27 black holes in our sample of 72 are new measurements and 18 masses are updates of previous values from improved data and/or modeling. Our present sample includes updated distances to 44 galaxies.

We have presented revised fits for the $M_\bullet$–σ, $M_\bullet$–L, and $M_\bullet$–$M_{\rm bulge}$ relations of our updated sample (Table 2 and Figures 1–3). Each relation is fit as a power law: $\log_{10}(M_\bullet) = \alpha + \beta \log_{10}(X)$. Our best fit to the full sample of 72 galaxies with velocity dispersion measurements ($X \equiv \sigma/200\,{\rm km\,s^{-1}}$) is $\alpha = 8.32 \pm 0.05$ and $\beta = 5.64 \pm 0.31$. A quadratic fit to the $M_\bullet$–σ relation with an additional term $\beta_2\,[\log_{10}(X)]^2$ gives $\beta_2 = 1.68 \pm 1.82$ and does not decrease the intrinsic scatter in $M_\bullet$. Including 92 additional upper limits for $M_\bullet$ decreases the intercept but does not change the slope: $\alpha = 8.15 \pm 0.05$ and $\beta = 5.58 \pm 0.30$.

For the 44 early-type galaxies with reliable V-band luminosity measurements ($X \equiv L_V/10^{11}\,L_\odot$), we find $\alpha = 9.23 \pm 0.10$ and $\beta = 1.11 \pm 0.13$. For the 35 early-type galaxies with dynamical measurements of the bulge stellar mass ($X \equiv M_{\rm bulge}/10^{11}\,M_\odot$), we find $\alpha = 8.46 \pm 0.08$ and $\beta = 1.05 \pm 0.11$.

We have also examined the black hole scaling relations for different subsamples of galaxies. When the galaxies are separated into early and late types and fit individually for the $M_\bullet$–σ relation, we find similar slopes of $\beta = 5.20 \pm 0.36$ (early types) and 5.06 ± 1.16 (late types). The intercepts, however, differ significantly: $\alpha = 8.39 \pm 0.06$ for the early types, a factor of $\sim$2 higher than $\alpha = 8.07 \pm 0.21$ for the late types. The steep global slope of 5.64 is therefore largely an effect of combining different galaxy types, each of which obeys a shallower $M_\bullet$–σ relation and different intercepts.

When the early-type galaxies are further divided into two subsamples based on their inner surface brightness profiles, the resulting $M_\bullet$–σ relation has a significantly larger intercept for the core galaxies than the power-law galaxies (Table 2 and Figure 4(a)). The slopes of the $M_\bullet$–L and $M_\bullet$–$M_{\rm bulge}$ relations do not show statistically significant differences between core and power-law galaxies, but $M_\bullet$ follows L and $M_{\rm bulge}$ more tightly in core galaxies than power-law galaxies (Table 2).

In the literature, the exact value of the $M_\bullet$–σ slope has been much debated by observers and regarded by theorists as a key discriminator for models of the assembly and growth of supermassive black holes and their host galaxies. We suggest that the individual observed $M_\bullet$–σ relations for the early- and late-type galaxies provide more meaningful constraints on theoretical models than the global relation. After all, these two types of galaxies are formed via different processes. Superficially, our measurement of $\beta = 5.64 \pm 0.32$ for the global $M_\bullet$–σ relation favors thermally driven wind models that predict $\beta \sim 5$ (e.g., Silk & Rees 1998) over momentum-driven wind models with $\beta \sim 4$ (e.g., Fabian 1999). However, the intercept of the empirical $M_\bullet$–σ relation is substantially higher than intercepts derived from thermally driven wind models (e.g., King 2010a, 2010b).

For the subsamples, the early-type galaxies give $\beta > 4.0$ with 99.96% confidence ($\Delta\chi^2 = 11.3$ for $\epsilon_0 = 0.34$) and $\beta > 4.5$ with 97% confidence ($\Delta\chi^2 = 3.8$), whereas the late-type and power-law galaxy subsamples are each consistent with $\beta = 4.0$ ($\Delta\chi^2 < 1$). Core galaxies exceed $\beta = 4.0$ with marginal significance ($\Delta\chi^2 = 1.1$) and are consistent with $\beta = 4.5$. Including central kinematics in the definition of σ further erodes the significance of high β for the early-type and core galaxy subsamples. More robust black hole measurements and more sophisticated theoretical models taking into account of galaxy types and environment (e.g., Zubovas & King 2012) are needed before stronger constraints can be obtained.

The intrinsic scatter in $M_\bullet$ plotted in Figure 5 for different intervals of σ, L, and $M_{\rm bulge}$ serves as an independent test for theoretical models of black hole and galaxy growth. Our data set shows decreasing scatter in $M_\bullet$ with increasing σ. However, there are currently insufficient data to probe the 30–100 ${\rm km\,s^{-1}}$ range, where scatter in $M_\bullet$ could identify the initial formation mechanism for massive black holes (Volonteri et al. 2008; Volonteri & Natarajan 2009). Theoretical models of hierarchical mergers in Λ cold dark matter cosmology predict that scatter in $M_\bullet$ should decline steadily with increasing stellar mass ($M_\star$), even when $M_\bullet$ and $M_\star$ are initially uncorrelated (Malbon et al. 2007; Peng 2007; Hirschmann et al. 2010; Jahnke & Macciò 2011). The semi-analytic models by Malbon et al. (2007), for instance, predict that black holes with present-day masses $>10^8\,M_\odot$ have gained most of their mass via black hole–black hole mergers, yielding extremely low scatter ($\epsilon_0 \sim 0.1$) at the upper end of the $M_\bullet$–$M_{\rm bulge}$ relation. More recent models by Jahnke & Macciò (2011) use fully decoupled prescriptions for star formation and black hole growth, and attain a more realistic amount of scatter on average, yet these models still exhibit decreasing scatter as $M_{\rm bulge}$ increases from $\sim 10^9\,M_\odot$ to $\sim 10^{11.5}\,M_\odot$. In comparison, we observe nearly constant scatter from $M_{\rm bulge} \sim 10^{11}\,M_\odot$ to $10^{12}\,M_\odot$, beyond the highest bulge masses produced in the Jahnke & Macciò (2011) models.

Our final comment is that investigations using the $M_\bullet$–σ correlation should consider the definition of σ, i.e., whether it is measured from an inner radius of zero or $r_{\rm inf}$. We find that both definitions yield similar amounts of scatter in the $M_\bullet$–σ relation (Table 2), so neither has a clear advantage for predicting $M_\bullet$. Excluding data within $r_{\rm inf}$ corresponds more closely to cases where $r_{\rm inf}$ is unresolved, such as seeing-limited galaxy surveys, high-redshift observations, or numerical simulations with limited spatial resolution. From a theoretical perspective, the evolutionary origin of an $M_\bullet$–σ relation and the immediate effects of gravity may warrant separate consideration. On the other hand, the total gravitational potential of a galaxy includes its black hole. Our test of how redefining σ alters the $M_\bullet$–σ relation has only considered 12 galaxies for which data within $r_{\rm inf}$ contribute prominently to the spatially integrated velocity dispersion. At present, the full sample of $M_\bullet$ and σ measurements comprises a heterogeneous selection of kinematic data. Rather than advocating a particular definition, we wish to call attention to the nuances of interpreting the $M_\bullet$–σ relation and encourage future investigators to consider their options carefully.

As this manuscript was being finalized, van den Bosch et al. (2012) reported a measurement of $M_\bullet = 1.7 \pm 0.3 \times 10^{10}\, M_\odot$ in NGC 1277. They reported $\sigma = 333\,\mathrm{km\,s^{-1}}$ for data between r_{inf} and r_{eff}, and $M_{\mathrm{bulge}} = 1.2 \pm 0.4 \times 10^{11}\, M_\odot$; the latter measurement suggests that NGC 1277 lies two orders of magnitude above the mean $M_\bullet$–M_{bulge} relation. Adding NGC 1277 to our 72-galaxy sample changes our global power-law fit to the $M_\bullet$–σ relation only slightly: $\alpha = 8.33 \pm 0.05$, $\beta = 5.73 \pm 0.32$, and $\epsilon_0 = 0.39$ (from MPFITEXY). Our global fit to $M_\bullet(M_{\mathrm{bulge}})$ for 36 galaxies including NGC 1277 yields $\alpha = 8.51 \pm 0.09$, $\beta = 1.05 \pm 0.13$, and $\epsilon_0 = 0.44$.

Dynamical measurements of $M_\bullet$ require substantial observational resources and careful analysis, and are often published individually. Nonetheless, recent and ongoing efforts are rapidly expanding the available $M_\bullet$ measurements and revising the empirical black hole scaling relations. Our online database[4] aims to provide all researchers easy access to frequently updated compilation of supermassive black holes with direct dynamical mass measurements and their host galaxy properties. Updated scaling relations can be used to estimate $M_\bullet$ more accurately in individual galaxies. This can improve our knowledge of Eddington rates and spectral energy distributions for accreting black holes, as well as time and distance scales for tidal disruption events. Moreover, the $M_\bullet$–σ relation for quiescent black holes has been used to normalize the black hole masses obtained from reverberation mapping studies of active galaxies (Onken et al. 2004; Woo et al. 2010; Park et al. 2012). This important calibration could be improved by addressing morphology biases in the reverberation mapping samples and the $M_\bullet$–σ relations for different galaxy types.

This work is supported in part by NSF AST-1009663. N.J.M. is supported by the Beatrice Watson Parrent Fellowship. We thank Karl Gebhardt, Tod Lauer, and John Blakeslee for useful discussions, and Michael Reed for help with the data table and compilation. We thank the anonymous referee for constructive comments on our original manuscript.

REFERENCES

Atkinson, J. W., Collett, J. L., Marconi, A., et al. 2005, MNRAS, 359, 504
Baes, M., Buyle, P., Hau, G. K. T., & Dejonghe, H. 2003, MNRAS, 341, L44
Barth, A. J., Sarzi, M., Rix, H.-W., et al. 2001, ApJ, 555, 685
Beifiori, A., Courteau, S., Corsini, E. M., & Zhu, Y. 2012, MNRAS, 419, 2497 (B12)
Beifiori, A., Sarzi, M., Corsini, E. M., et al. 2009, ApJ, 692, 856
Bender, R., Kormendy, J., Bower, G., et al. 2005, ApJ, 631, 280
Bernardi, M., Hyde, J. B., Sheth, R. K., Miller, C. J., & Nichol, R. C. 2007, AJ, 133, 1741
Blakeslee, J. P., Cantiello, M., Mei, S., et al. 2010, ApJ, 724, 657
Blakeslee, J. P., Jordán, A., Mei, S., et al. 2009, ApJ, 694, 556
Bogdán, Á., Forman, W. R., Kraft, R. P., et al. 2012, ApJ, 755, 25
Bower, G. A., Green, R. F., Bender, R., et al. 2001, ApJ, 550, 75
Boylan-Kolchin, M., Ma, C.-P., & Quataert, E. 2006, MNRAS, 369, 1081
Braatz, J. A., Reid, M. J., Humphreys, E. M. L., et al. 2010, ApJ, 718, 657
Burkert, A., & Tremaine, S. 2010, ApJ, 720, 516
Cappellari, M., Bacon, R., Bureau, M., et al. 2006, MNRAS, 366, 1126
Cappellari, M., Neumayer, N., Reunanen, J., et al. 2009, MNRAS, 394, 660
Cappellari, M., Verolme, E. K., van der Marel, R. P., et al. 2002, ApJ, 578, 787
Conroy, C., & van Dokkum, P. G. 2012, ApJ, 760, 71
Cretton, N., & van den Bosch, F. C. 1999, ApJ, 514, 704
Dalla Bontà, E., Ferrarese, L., Corsini, E. M., et al. 2009, ApJ, 690, 537
Davies, R. I., Thomas, J., Genzel, R., et al. 2006, ApJ, 646, 754
de Francesco, G., Capetti, A., & Marconi, A. 2008, A&A, 479, 355
Devereux, N., Ford, H., Tsvetanov, Z., & Jacoby, G. 2003, AJ, 125, 1226
D'Onofrio, M., Zaggia, S. R., Longo, G., Caon, N., & Capaccioli, M. 1995, A&A, 296, 319
Emsellem, E., Dejonghe, H., & Bacon, R. 1999, MNRAS, 303, 495
Faber, S. M., Tremaine, S., Ajhar, E. A., et al. 1997, AJ, 114, 1771
Fabian, A. C. 1999, MNRAS, 308, L39
Ferrarese, L. 2002, ApJ, 578, 90
Ferrarese, L., Côté, P., Jordán, A., et al. 2006, ApJS, 164, 334
Ferrarese, L., & Ford, H. C. 1999, ApJ, 515, 583
Ferrarese, L., Ford, H. C., & Jaffe, W. 1996, ApJ, 470, 444
Ferrarese, L., & Merritt, D. 2000, ApJL, 539, L9
Gebhardt, K., Adams, J., Richstone, D., et al. 2011, ApJ, 729, 119
Gebhardt, K., Bender, R., Bower, G., et al. 2000, ApJL, 539, L13
Gebhardt, K., Lauer, T. R., Pinkney, J., et al. 2007, ApJ, 671, 1321
Gebhardt, K., Richstone, D., Tremaine, S., et al. 2003, ApJ, 583, 92
Gebhardt, K., & Thomas, J. 2009, ApJ, 700, 1690
Ghez, A. M., Salim, S., Weinberg, N. N., et al. 2008, ApJ, 689, 1044
Gillessen, S., Eisenhauer, F., Trippe, S., et al. 2009, ApJ, 692, 1075
Glass, L., Ferrarese, L., Côté, P., et al. 2011, ApJ, 726, 31
Graham, A. W. 2007, MNRAS, 379, 711
Graham, A. W. 2008, PASA, 25, 167
Graham, A. W. 2012, ApJ, 746, 113
Graham, A. W., Colless, M. M., Busarello, G., Zaggia, S., & Longo, G. 1998, A&AS, 133, 325
Graham, A. W., & Driver, S. P. 2007, ApJ, 655, 77
Graham, A. W., Erwin, P., Caon, N., & Trujillo, I. 2001, ApJL, 563, L11
Graham, A. W., Onken, C. A., Athanassoula, E., & Combes, F. 2011, MNRAS, 412, 2211
Greene, J. E., Peng, C. Y., Kim, M., et al. 2010, ApJ, 721, 26
Greenhill, L. J., Booth, R. S., Ellingsen, S. P., et al. 2003, ApJ, 590, 162
Gültekin, K., Richstone, D. O., Gebhardt, K., et al. 2009a, ApJ, 698, 198 (G09)
Gültekin, K., Richstone, D. O., Gebhardt, K., et al. 2009b, ApJ, 695, 1577
Gültekin, K., Richstone, D. O., Gebhardt, K., et al. 2011, ApJ, 741, 38
Häring, N., & Rix, H.-W. 2004, ApJL, 604, L89
Harris, G. L. H., & Harris, W. E. 2011, MNRAS, 410, 2347
Herrnstein, J. R., Moran, J. M., Greenhill, L. J., & Trotter, A. S. 2005, ApJ, 629, 719
Hirschmann, M., Khochfar, S., Burkert, A., et al. 2010, MNRAS, 407, 1016
Houghton, R. C. W., Magorrian, J., Sarzi, M., et al. 2006, MNRAS, 367, 2
Hu, J. 2008, MNRAS, 386, 2242
Hu, J. 2009, arXiv:0908.2028
Isobe, T., Feigelson, E. D., & Nelson, P. I. 1986, ApJ, 306, 490
Jahnke, K., & Macciò, A. V. 2011, ApJ, 734, 92
Jardel, J. R., Gebhardt, K., Shen, J., et al. 2011, ApJ, 739, 21
Kelly, B. C. 2007, ApJ, 665, 1489
King, A. R. 2010a, MNRAS, 402, 1516
King, A. R. 2010b, MNRAS, 408, L95
Kondratko, P. T., Greenhill, L. J., & Moran, J. M. 2008, ApJ, 678, 87
Kormendy, J., & Bender, R. 2009, ApJL, 691, L142
Kormendy, J., & Bender, R. 2011, Natur, 469, 377
Kormendy, J., Bender, R., & Cornell, M. E. 2011, Natur, 469, 374
Kormendy, J., & Gebhardt, K. 2001, in AIP Conf. Proc. 586, 20th Texas Symposium on Relativistic Astrophysics, ed. J. C. Wheeler & H. Martel (Melville, NY: AIP), 363
Kormendy, J., & Richstone, D. 1995, ARA&A, 33, 581
Krajnović, D., McDermid, R. M., Cappellari, M., & Davies, R. L. 2009, MNRAS, 399, 1839
Kuo, C. Y., Braatz, J. A., Condon, J. J., et al. 2011, ApJ, 727, 20
Lauer, T. R., Faber, S. M., Richstone, D., et al. 2007a, ApJ, 662, 808
Lauer, T. R., Gebhardt, K., Faber, S. M., et al. 2007b, ApJ, 664, 226
Lauer, T. R., Tremaine, S., Richstone, D., & Faber, S. M. 2007c, ApJ, 670, 249
Lavalley, M. P., Isobe, T., & Feigelson, E. D. 1992, BAAS, 24, 839
Lodato, G., & Bertin, G. 2003, A&A, 398, 517
Magorrian, J., Tremaine, S., Richstone, D., et al. 1998, AJ, 115, 2285
Malbon, R. K., Baugh, C. M., Frenk, C. S., & Lacey, C. G. 2007, MNRAS, 382, 1394
Marconi, A., & Hunt, L. K. 2003, ApJL, 589, L21
McConnell, N. J., Ma, C.-P., Gebhardt, K., et al. 2011a, Natur, 480, 215
McConnell, N. J., Ma, C.-P., Graham, J. R., et al. 2011b, ApJ, 728, 100
McConnell, N. J., Ma, C.-P., Murphy, J. D., et al. 2012, ApJ, 756, 179
McLure, R. J., & Dunlop, J. S. 2002, MNRAS, 331, 795
McLure, R. J., & Dunlop, J. S. 2004, MNRAS, 352, 1390
Merritt, D., & Ferrarese, L. 2001, ApJ, 547, 140
Neumayer, N., Cappellari, M., Reunanen, J., et al. 2007, ApJ, 671, 1329
Novak, G. S., Faber, S. M., & Dekel, A. 2006, ApJ, 637, 96
Nowak, N., Saglia, R. P., Thomas, J., et al. 2008, MNRAS, 391, 1629
Nowak, N., Saglia, R. P., Thomas, J., et al. 2007, MNRAS, 379, 909

[4] http://blackhole.berkeley.edu

Nowak, N., Thomas, J., Erwin, P., et al. 2010, MNRAS, 403, 646
Onken, C. A., Ferrarese, L., Merritt, D., et al. 2004, ApJ, 615, 645
Park, D., Kelly, B. C., Woo, J.-H., & Treu, T. 2012, ApJS, 203, 6
Peng, C. Y. 2007, ApJ, 671, 1098
Pinkney, J., Gebhardt, K., Bender, R., et al. 2003, ApJ, 596, 903
Pu, S. B., Saglia, R. P., Fabricius, M. H., et al. 2010, A&A, 516, A4
Rusli, S. P. 2012, PhD thesis, Ludwig Maximilians Universität, München
Rusli, S. P., Thomas, J., Erwin, P., et al. 2011, MNRAS, 410, 1223
Sadoun, R., & Colin, J. 2012, MNRAS, 426, L51
Sani, E., Marconi, A., Hunt, L. K., & Risaliti, G. 2011, MNRAS, 413, 1479
Sarzi, M., Rix, H.-W., Shields, J. C., et al. 2001, ApJ, 550, 65
Schulze, A., & Gebhardt, K. 2011, ApJ, 729, 21
Shen, J., & Gebhardt, K. 2010, ApJ, 711, 484
Silk, J., & Rees, M. J. 1998, A&A, 331, L1
Simien, F., & Prugniel, P. 2000, A&AS, 145, 263
Spolaor, M., Forbes, D. A., Hau, G. K. T., Proctor, R. N., & Brough, S. 2008, MNRAS, 385, 667
Tonry, J. L., Dressler, A., Blakeslee, J. P., et al. 2001, ApJ, 546, 681
Tremaine, S., Gebhardt, K., Bender, R., et al. 2002, ApJ, 574, 740
Tundo, E., Bernardi, M., Hyde, J. B., Sheth, R. K., & Pizzella, A. 2007, ApJ, 663, 53
van den Bosch, R. C. E., & de Zeeuw, P. T. 2010, MNRAS, 401, 1770
van den Bosch, R. C. E., Gebhardt, K., Gültekin, K., et al. 2012, Natur, 491, 729
van der Marel, R. P., & van den Bosch, F. C. 1998, AJ, 116, 2220
Verolme, E. K., Cappellari, M., Copin, Y., et al. 2002, MNRAS, 335, 517
Vilardell, F., Jordi, C., & Ribas, I. 2007, A&A, 473, 847
Volonteri, M., Lodato, G., & Natarajan, P. 2008, MNRAS, 383, 1079
Volonteri, M., & Natarajan, P. 2009, MNRAS, 400, 1911
Volonteri, M., Natarajan, P., & Gültekin, K. 2011, ApJ, 737, 50
Walsh, J. L., Barth, A. J., & Sarzi, M. 2010, ApJ, 721, 762
Walsh, J. L., van den Bosch, R. C. E., Barth, A. J., & Sarzi, M. 2012, ApJ, 753, 79
Williams, M. J., Bureau, M., & Cappellari, M. 2010, MNRAS, 409, 1330
Wold, M., Lacy, M., Käufl, H. U., & Siebenmorgen, R. 2006, A&A, 460, 449
Woo, J.-H., Treu, T., Barth, A. J., et al. 2010, ApJ, 716, 269
Wyithe, J. S. B. 2006a, MNRAS, 365, 1082
Wyithe, J. S. B. 2006b, MNRAS, 371, 1536
Zasov, A. V., Petrochenko, L. N., & Cherepashchuk, A. M. 2005, ARep, 49, 362
Zubovas, K., & King, A. R. 2012, MNRAS, 426, 2751